New Plane Shear Flows

Thesis by

Andrew Conley

In Partial Fulfillment of the Requirements

for the Degree of

Doctor of Philosophy

California Institute of Technology

Pasadena, California

1994

(Submitted June 9, 1993)

Acknowledgments

I wish to thank my advisor, Herb Keller, who has always wished the best for me and has expected the most from me. I appreciate the kind help of Professor Saffman, who asked me many of the questions which led to this work. I would also like to thank Fausto Milinazzo for many lively discussions of the material.

I could not have done the work of this thesis without the support of my parents, David and Sharon Conley, and my friend, Laura Brockman.

This work was supported in part by the NSF under Cooperative Agreement No. CCR-9120008 and the U.S. Department of Energy under Contract Nos. DE-AA03-76SF00767 and DE-FG03-89ER25073. The government has certain rights in this material.

Abstract

A classical problem in fluid dynamics is the study of the stability of plane Couette flow. This flow experimentally sustains turbulence for Reynolds numbers greater than 1440 ± 40 (see [10],[5]). (The Reynolds number is based on channel width and wall velocity difference). Since plane Couette flow is linearly stable for all Reynolds numbers, obtaining non-trivial mathematical solutions to the plane Couette flow equations is difficult. However, M. Nagata [6] finds a non-trivial numerical solution of the plane Couette flow equations at low Reynolds number. We confirm these solutions. We compute the minimum Reynolds number at which they exist. We study their stability. We also study the effect of a Coriolis force on plane Poiseuille flow.

Contents

List of Figures

List of Tables

Chapter 1

Introduction

A long standing problem in fluid mechanics is understanding the mechanisms or processes by which a laminar flow becomes turbulent. This problem has been studied in many specific cases. We will concentrate on the case of an incompressible viscous fluid between infinite parallel plates. There are two canonical examples of this special case. In one example, the plates shear past one another with constant velocities. This example is called plane Couette flow. For plane Couette flow, we define the Reynolds number to be the velocity difference of the plates times the distance between the plates divided by the viscosity of the fluid.

The other canonical example is that of plane Poiseuille flow. This is the flow between stationary plates with an external driving force parallel to the plates.

Experimentally, plane Couette flow sustains turbulence for large enough Reynolds number ($Re > Re_t = 1440 \pm 40$) (see [10]). For Reynolds numbers

less than the transition number ($Re < Re_t$) the flow becomes a laminar flow with the velocity depending only on the distance from each plate. Theoretically and numerically, all studies seem to imply linear stability of this laminar flow for all Reynolds numbers (see [9] [2]). The lack of bifurcations or other known solutions for plane Couette flow make study of this transition difficult.

In contrast, Taylor–Couette flow bifurcates to other flows for large enough Reynolds numbers. Taylor–Couette flow is the flow between infinitely long coaxial cylinders. If the gap between the cylinders is small compared to the average radius of the cylinders, Taylor–Couette flow is approximated by plane Couette flow in a rotating channel. This limit is discussed in Appendix A

M. Nagata (see [6],[7],[8]) finds new solutions to plane Couette flow by studying plane Couette flow in a channel rotating with speed Ω about the z axis (see Figure 1.1). He finds bifurcations to two–dimensional solutions. These solutions look like Taylor vortices in Taylor–Couette flow. The axis of each vortex is aligned with the velocity of the bounding plates. When the rotation is further increased, he finds another bifurcation. The new solution bifurcating from the vortex solution has variation in all three directions. It looks like wavy Taylor vortices in Taylor Couette flow. The rotation, Ω, can be decreased to zero while retaining the three–dimensional structure of the solutions. These solutions are poorly resolved due to Nagata's use of series of Chandrasekhar functions to approximate the flow fields in the direction normal to the plates.

We reformulate the problem in terms of Chebyshev polynomials instead of Chandrasekhar functions. These polynomials provide much better resolved

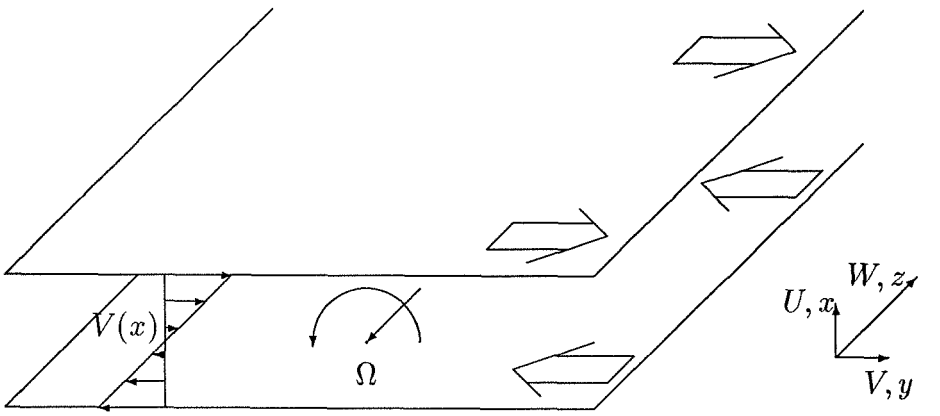

Figure 1.1: We study flow between infinite parallel shearing plates. The plates are tumbling with angular velocity, Ω. The linear velocity profile, $v(x)$, seems to be (linearly) stable for all shear rates.

solutions. We also exploit a symmetry of the solution allowing us to do most of the calculation on workstations (avoiding the need for time on a supercomputer.) While this limits the types of solutions we can obtain, the use of the symmetry increases the speed and accuracy of the solutions. We study the dependence of these solutions on other parameters of the problem using the path following techniques of H. B. Keller [4]. These methods allow us to accurately locate bifurcation points and to find the minimum Reynolds number at which these solutions exist.

This minimum Reynolds number ($Re = 467$) is about one third the Reynolds number at which the flow experimentally sustains turbulence. In an attempt to clarify this difference, we study the linear stability of this flow to all disturbances having the same symmetry as the solution. The resulting

spectrum implies that some of the solutions may be stable.

We study several aspects of the problem. First we obtain the three–dimensional solutions confirming the results of Nagata. Studying these solutions allows us to find a symmetry. By exploiting these symmetries, we further resolve the solution. Next we study the dependence of the solution on several parameters of the problem. Lastly, we compute the eigenvalues of the underlying linear problem in order to examine the linear stability for these flows.

In Appendix A we relate the equations which Nagata studies to the equations describing Taylor–Couette flow. The cylinders are rotating with an average angular velocity Ω. The gap between them is a and their average radius is b. In the limit $a/b \to 0$, the equations for a fluid between concentric cylinders reduce to the equations satisfied by a fluid between parallel plates with a Coriolis force (resulting from the rotating coordinate frame.)

We define

$$\vec{U}(x,y,z,t) = \begin{pmatrix} U(x,y,z,t) \\ V(x,y,z,t) \\ W(x,y,z,t) \end{pmatrix}$$

to be the velocity of the flow at time t and at location (x,y,z) (see Figure 1.1). We define $P(x,y,z,t)$ to be the pressure of the flow. The Navier–Stokes equation for flow between parallel plates with a Coriolis force are as follows:

$$\frac{\partial \vec{U}}{\partial t} = -\,\mathrm{Re}\,(\vec{U}\cdot\vec{\nabla})\vec{U} + \nabla^2\vec{U} - \vec{\nabla}P + 2\Omega(\hat{z}\times\vec{U}), \tag{1.1}$$

$$0 = \vec{\nabla}\cdot\vec{U}. \tag{1.2}$$

The solutions of these equations are required to be solutions which satisfy no

slip boundary conditions at the plates which are at $x = \pm 1/2$ and periodic boundary conditions in the x and z coordinate directions parallel to the plates:

$$\vec{U}(-\frac{1}{2}, y, z, t) = +\frac{V_0}{2}\hat{y}, \tag{1.3}$$

$$\vec{U}(\frac{1}{2}, y, z, t) = -\frac{V_0}{2}\hat{y}, \tag{1.4}$$

$$\vec{U}(x, y + \lambda_y, z, t) = \vec{U}(x, y, z, t), \tag{1.5}$$

$$P(x, y + \lambda_y, z, t) = P(x, y, z, t) + \lambda_y F_y, \tag{1.6}$$

$$\vec{U}(x, y, z + \lambda_z, t) = \vec{U}(x, y, z, t), \tag{1.7}$$

$$P(x, y, z + \lambda_z, t) = P(x, y, z, t) + \lambda_z F_z. \tag{1.8}$$

The parameters, F_y and F_z, are external forces on the flow.

We seek traveling wave solutions to equations (1.1) through (1.8), where c_y and c_z are the speeds of the traveling waves in the y and z directions respectively:

$$\vec{U}(x, y, z, t) = \vec{V}(x, y - c_y t, z - c_z t),$$

$$P(x, y, z, t) - yF_y - zF_z = p(x, y - c_y t, z - c_z t),$$

$$\vec{V}(x, y, z) = \begin{pmatrix} u(x, y, z) \\ v(x, y, z) \\ w(x, y, z) \end{pmatrix}.$$

As a result, we require $\vec{V}(x,y,z)$ and $p(x,y,z)$ to satisfy the following equations:

$$\begin{aligned} 0 &= -\,\mathrm{Re}\,(\vec{V}\cdot\vec{\nabla})\vec{V} + \nabla^2\vec{V} - \vec{\nabla}p + 2\Omega(\hat{z}\times\vec{V}) \\ &\quad + F_y\hat{y} + F_z\hat{z} + c_y\partial_y\vec{V} + c_z\partial_z\vec{V}, \qquad (1.9) \\ 0 &= \vec{\nabla}\cdot\vec{V}, \qquad (1.10) \end{aligned}$$

$$\begin{aligned} \vec{V}(-\frac{1}{2},y,z) &= +\frac{V_0}{2}\hat{y}, \qquad (1.11) \\ \vec{V}(\frac{1}{2},y,z) &= -\frac{V_0}{2}\hat{y}, \qquad (1.12) \\ \vec{V}(x,y+\lambda_y,z) &= \vec{V}(x,y,z), \qquad (1.13) \\ p(x,y+\lambda_y,z) &= p(x,y,z), \qquad (1.14) \\ \vec{V}(x,y,z+\lambda_z) &= \vec{V}(x,y,z), \qquad (1.15) \\ p(x,y,z+\lambda_z) &= p(x,y,z). \qquad (1.16) \end{aligned}$$

These equations have two well–known special cases. In the case of shearing plates with no rotation and no external forcing ($V_0 = 1$, $\Omega = 0$, $F_y = 0$, $F_z = 0$) plane Couette flow is one solution. The other special case is that of plane Poiseuille flow for which $V_0 = 0$, $\Omega = 0$, $F_y = 2$, $F_z = 0$. We concentrate mainly on the case of plane Couette flow with Ω sometimes varying from zero.

We break our study of these equations into three parts. In Chapter 2 we describe our formulation of the problem. We use a truncated Fourier series to approximate the velocity and pressure fields in the periodic directions. In the non-periodic (cross–channel) direction we use Chebyshev polynomials. We

define the shear stress (τ) of the fluid on the bounding plate. We use τ as a parameter which allows us to follow folds and pass folds which are present in other parameterizations. We describe our implementation of path following. We describe our phase constraints (which are necessary due to the periodic boundary conditions) and how we take advantage of an observed symmetry to eliminate half the variables.

In Chapter 3 we study the results of this formulation when there is no external forcing. We also discuss the bifurcations and the (linear) stability of various branches of solutions. We study the spectrum resulting from the linearization of the Navier–Stokes equations at various points along these branches. We also describe the method and results of locating the minimum Reynolds number for which the bifurcating solutions exist.

In Chapter 4 we study how the three–dimensional solution varies with forcing. We also describe the results of our study of Poiseuille flow. We find a first bifurcation from simple Poiseuille flow to a flow which has variation in the z direction. We do not find a 3-dimensional flow (corresponding to wavy vortices.)

Chapter 2

Formulation of the Problem

After a brief review of Galerkin and Tau methods, we describe our approximation of the velocity and pressure fields. Then we discuss our method for following paths of solutions. Lastly, we discuss some implementation issues.

2.1 Review of Galerkin and Tau Methods

It will be easier to discuss our approximations of the Navier-Stokes equations if we first review Galerkin and tau spectral methods. For a more thorough study of these methods, see *Numerical Analysis of Spectral Methods: Theory and Applications* by D. Gottlieb and S. A. Orszag [3]. For a study of applications of spectral methods to the Navier Stokes equations, see *Spectral Methods in Fluid Dynamics* by Canuto, Hussaini, Quarteroni, and Zang [1]

The difference between tau and Galerkin methods lies in their treatment of boundary conditions. In a Galerkin method, the basis functions for the

expansion satisfy the boundary conditions. For example, if $F(u(x)) = 0$ is a differential equation and we require $u(x)$ to be periodic, say:

$$u(x + \pi) = u(x - \pi),$$

then we can approximate u by a truncated fourier series,

$$\hat{u} = \sum_{n=-N}^{N} u_n e^{inx}.$$

We require the following projections of the residual, $F(\hat{u})$, to be zero:

$$\int_{-\pi}^{\pi} e^{inx} F(\hat{u}) dx = 0,$$

$$\forall n \in \{-N, -N+1, ...N\}.$$

The boundary conditions are satisfied by $\hat{u}(x)$ and we have $2N+1$ projection conditions to determine the coefficients $u_n, -N \leq n \leq N$.

In contrast, the basis functions of a tau method do not necessarily satisfy the boundary conditions. For example, if $F(u(x)) = 0$ is a differential equation and we require $u(x)$ to satisfy Dirichlet boundary conditions, say:

$$u(-1) = 0 = u(1),$$

we can approximate the solution u by a truncated Chebyshev series,

$$\hat{u} = \sum_{n=0}^{N} u_n T_n(x).$$

Since the Chebyshev polynomials do not satisfy the required Dirichlet boundary conditions, we require $\hat{u}$ to satisfy them:

$$\sum_{n=0}^{N} u_n (-1)^n = 0,$$

$$\sum_{n=0}^{N} u_n = 0.$$

The boundary conditions provide two equations for the $N + 1$ unknowns.

Since we cannot in general require the residual, $F(\hat{u})$, to be zero and we already have imposed two equations for the unknowns coming from the boundary conditions, we only require that the first $N-1$ projections of the residual to be zero as follows:

$$\int_{-1}^{1} \frac{T_n(x)F(\hat{u}(x))}{\sqrt{1-x^2}}dx = 0,$$
$$\forall n \in \{0, 1, ...N-2\}.$$

In this way we get $N+1$ equations for the unknown coefficients $u_n, 0 \leq n \leq N$.

2.2 Approximation of Velocity and Pressure Fields

We use a Galerkin method in the y and z directions and a slight modification of the tau method in the x direction to approximate the velocity and pressure fields. First, however, we introduce the basis functions for the expansion.

We use the two wave numbers,

$$\alpha_y = \frac{2\pi}{\lambda_y},$$
$$\alpha_z = \frac{2\pi}{\lambda_z},$$

in our basis functions. The wave numbers are defined in terms of the periodicities (λ_y and λ_z) appearing in the periodic boundary conditions (1.13)–(1.16). We use these wave numbers and the Chebyshev polynomials, $T_l(x)$, to construct the basis functions,

$$C_{l,m,n}(x, y, z) = T_l(2x)\cos(m\alpha_y y + n\alpha_z z),$$

$$S_{l,m,n}(x,y,z) = T_l(2x)\sin(m\alpha_y y + n\alpha_z z).$$

We seek the approximate solutions,

$$\begin{pmatrix} u_a \\ v_a \\ w_a \end{pmatrix} = \vec{V}_a \approx \vec{V},$$

$$p_a \approx p,$$

of equations (1.9)–(1.16). Each of the scalar fields, u_a, v_a, w_a, and p_a, are truncated series expansions of the form,

$$\begin{aligned} q_a(x,y,z) &= \sum_{l=0}^{L} 2Q_{l,0,0}C_{l,0,0}(x,y,z) \\ &\quad + \sum_{l=0}^{L}\sum_{n=1}^{N} Q_{l,0,n}C_{l,0,n}(x,y,z) - Q'_{l,0,n}S_{l,0,n}(x,y,z) \\ &\quad + \sum_{l=0}^{L}\sum_{m=1}^{M}\sum_{n=-N}^{N} Q_{l,m,n}C_{l,m,n}(x,y,z) - Q'_{l,m,n}S_{l,m,n}(x,y,z), \end{aligned} \tag{2.1}$$

where q represents u, v, w, or p. This expansion has $(L+1)(1+2M)(1+2N)$ coefficients. As a result, we have approximated $\vec{V}$ and p with a total of $4(L+1)(1+2M)(1+2N)$ coefficients. It is much easier to work with this expansion in its complex form. In order to rewrite this series expansion, we define the following complex quantities:

$$q_{l,m,n} = \frac{1}{2}(Q_{l,m,n} + iQ'_{l,m,n}),$$

$$q_{l,-m,-n} = \frac{1}{2}(Q_{l,m,n} - iQ'_{l,m,n}),$$

$$Q'_{l,0,0} = 0$$

$$A_{l,m,n} = (C_{l,m,n} + iS_{l,m,n}) = T_l(2x)e^{i(m\alpha_y y + n\alpha_z z)}.$$

Then we can rewrite Eq. (2.2) in the form,

$$q_a(x,y,z) = \sum_{l=0}^{L} \sum_{m=-M}^{M} \sum_{n=-N}^{N} q_{l,m,n} A_{l,m,n}(x,y,z), \tag{2.2}$$

where q represents u, v, w, or p.

Since $\vec{V}_a$ and p_a satisfy the periodic boundary conditions in Eqs. (1.13)–(1.16), we can use a Galerkin method in the y and z directions. However, the approximate solutions $\vec{V}_a$ and p_a do not automatically satisfy the boundary conditions in Eqs. (1.11)– (1.12); therefore, we wish to use a tau method in the x direction. The tau method would be straightforward to implement if we had boundary conditions for the pressure at the plates, $p(-1/2, y, z)$ and $p(1/2, y, z)$. Instead, we use a slight modification of the tau method which is spelled out below.

In order to discuss our version of the tau method, we introduce the inner product,

$$\langle f, g \rangle = \int_{-\frac{1}{2}}^{\frac{1}{2}} \frac{dx}{\sqrt{1-4x^2}} \int_0^{\lambda_y} dy \int_0^{\lambda_z} dz f g.$$

We sometimes use the notation,

$$\langle f, \vec{g} \rangle.$$

Whenever we have a vector in the inner product, we mean the component-wise application of the inner product. In the following discussion, f will always be $S_{l,m,n}(x,y,z)$ or $C_{l,m,n}(x,y,z)$ and g will either be the right–hand side of Eq. (1.9) or Eq. (1.10). We define the set,

$$S(L,M,N)$$

to be the set of basis functions,

$$\begin{aligned} C_{l,0,0} \quad & \forall l \in \{0...L\}, \\ C_{l,0,n}, S_{l,0,n} \quad & \forall l \in \{0...L\}, n \in \{1...N\}, \\ C_{l,m,n}, S_{l,m,n} \quad & \forall l \in \{0...L\}, m \in \{1...M\}, n \in \{-N...N\}. \end{aligned}$$

We require $\vec{V}_a$ to satisfy the boundary conditions, (Eqs. (1.11)–(1.12)). We define the vector,

$$\vec{V}_{l,m,n} = \begin{pmatrix} u_{l,m,n} \\ v_{l,m,n} \\ w_{l,m,n} \end{pmatrix},$$

in terms of the expansion coefficients of the velocity fields, $u_{l,m,n}, v_{l,m,n}, w_{l,m,n}$, given in Eq. (2.2). Requiring $V_a(x,y,z)$ to satisfy Eqs. (1.11)–(1.12) leads to the equations,

$$\left.\begin{aligned} \textstyle\sum_{l=0}^{L} \vec{V}_{l,m,n} &= \begin{pmatrix} 0 \\ \frac{-V_0}{2}\delta_{m,0}\delta_{n,0} \\ 0 \end{pmatrix} \\ \textstyle\sum_{l=0}^{L}(-1)^l \vec{V}_{l,m,n} &= \begin{pmatrix} 0 \\ \frac{V_0}{2}\delta_{m,0}\delta_{n,0} \\ 0 \end{pmatrix} \end{aligned}\right\} \begin{aligned} &\forall m = 0, n \in \{0,...N\} \\ &\forall m \in \{1..M\}, n \in \{-N,...N\} \end{aligned} \tag{2.3}$$

Thus, the boundary conditions provide $6(1+2M)(1+2N)$ equations.

We require the following $(L-1)(1+2M)(1+2N)$ projections of the right–hand side of Eq. (1.9) to be zero:

$$\langle B, -\text{ Re }(\vec{V}_a \cdot \vec{\nabla})\vec{V}_a + \nabla^2 \vec{V}_a - \vec{\nabla} p_a + 2\Omega(\hat{z} \times \vec{V}_a) + c_y \partial_y \vec{V}_a + c_z \partial_z \vec{V}_a \rangle = 0 \tag{2.4}$$

$$\forall B \in S(L-2, M, N).$$

Since there are 3 equations for every projection, we have $3(L-1)(1+2M)(1+2N)$ equations for the unknown coefficients in the expansions of $\vec{V}_a$ and p_a. We also require the following $(L+1)(1+2M)(1+2N)$ projections of Eq. (1.10) to be zero:

$$\langle B, \vec{\nabla} \cdot \vec{V}_a \rangle = 0 \quad \forall B \in S(L, M, N). \tag{2.5}$$

We use $2(1+2M)(1+2N)$ more projections in Eqs. (2.5) than in Eqs. (2.4) since we have no boundary conditions for the pressure at the plates. A simple application of the tau method would have left us with fewer equations than unknowns.

Equations (2.3)–(2.5) provide $4(L+1)(1+2M)(1+2N)$ equations for the $4(L+1)(1+2M)(1+2N)$ unknown coefficients in the expansions $\vec{V}_a$ and p_a.

Compatibility Conditions

Unfortunately, the equations arising from our approximation scheme are linearly dependent. In particular, we note that the divergence condition, $\vec{\nabla} \cdot \vec{V} = 0$, and the boundary conditions on $\vec{V}$ have to satisfy a compatibility condition. An application of the divergence theorem gives us this relation as follows:

$$\begin{aligned} 0 &= \int_0^{\lambda_z} \int_0^{\lambda_y} \int_{-1/2}^{x} \vec{\nabla} \cdot \vec{V} dx dy dz \\ &= \int_0^{\lambda_z} \int_0^{\lambda_y} [u(x,y,z) - u(-1/2,y,z)] dy dz \\ &= \int_0^{\lambda_z} \int_0^{\lambda_y} u(x,y,z) dy dz. \end{aligned} \tag{2.6}$$

Hence, the average (over a periodic box) flux of fluid through any plane parallel to the plates must be zero. In particular, if we evaluate Eq. (2.6) at $x = 1/2$ we obtain the equation,

$$0 = \int_0^{\lambda_z} \int_0^{\lambda_y} u(1/2, y, z) dy dz. \tag{2.7}$$

While the boundary condition, $u(1/2, y, z) = 0$, satisfies the compatibility condition (2.7), this analysis shows a linear dependence of the boundary conditions (1.11,1.12) and the divergence condition (1.10). We discuss how this linear dependence shows up in our equations for the coefficients for the expansions $\vec{V}_a$ and p_a in the following.

In the system of equations (2.5), the divergence conditions,

$$\langle C_{l,0,0}, \vec{\nabla} \cdot \vec{V}_a \rangle = 0 \qquad \forall l \in \{0, ...L\}, \tag{2.8}$$

requires the coefficients of the expansion u_a (given in Eq. (2.2)),

$$u_{l,0,0} = 0 \qquad \forall l \in \{1, ...L\},$$

to be zero. Thus, the boundary conditions,

$$0 = \sum_{l=0}^{L} (-1)^l u_{l,0,0} = u_{0,0,0}, \tag{2.9}$$

$$0 = \sum_{l=0}^{L} u_{l,0,0} = u_{0,0,0}, \tag{2.10}$$

are not independent. We can satisfy Eq. (2.8), (2.9), and (2.10) by requiring the coefficients,

$$u_{0,0,0} = 0 \qquad \forall l \in \{0, ...L\}, \tag{2.11}$$

to be zero. This analysis allows us to satisfy the $(L+3)$ Eqs. (2.8), (2.9), and (2.10) with the $(L+1)$ Eqs. (2.11). We now need two independent equations to have as many equations as unknown coefficients.

The two independent equations come from recognizing that the pressure is not uniquely defined. The non-uniquenesses of the pressure are called spurious pressure modes (see [1]). These modes are defined as any non-zero $p_a(x,y,z)$ for which

$$\langle B, \vec{\nabla} p_a \rangle = 0 \qquad \forall B \in S(L,M,N).$$

In our formulation, there are two spurious pressure modes. One of the modes is the average value of the pressure. The other is a linear combination of the form,

$$\sum_{l=0}^{L} \alpha_l p_{l,0,0} T_l(x).$$

Instead of requiring these modes to be zero (which would provide the two independent equations), we note that the pressure coefficients,

$$p_{l,0,0} \qquad \forall l \in \{0, ...L\}$$

only appear in the equations,

$$\langle C_{l,0,0}, - \text{ Re } (\vec{V}_a \cdot \vec{\nabla}) u_a + \nabla^2 u_a - \partial_x p_a - 2\Omega v_a + c_y \partial_y u_a + c_z \partial_z u_a \rangle = 0, \quad (2.12)$$

$$\forall l \in \{0, ...L-2\}.$$

Equations (2.12) can be viewed as equations for the $p_{l,0,0}$ since Eqs. (2.12) are the only equations in which the coefficients, $p_{l,0,0}$, appear. By not enforcing Eq. (2.12), and not including the variables $p_{l,0,0}$ in the calculation, we have

removed $(L-1)$ equations and $(L+1)$ variables. While this leaves some components of the pressure field undetermined, the velocity field is unaffected by this removal of Eqs. (2.12) and pressure coefficients, $p_{l,0,0} \forall l \in \{0,..L\}$, from the calculation.

Summary of the Approximation

In summary, we solve $4(L+1)(1+2M)(1+2N)-(L+1)$ equations in the same number of unknowns. We represent these equations by the notation,

$$F(u,\lambda) = 0, \tag{2.13}$$

where F is the system of equations described in Eqs. (2.3,2.4,2.5,2.11) with the Eqs. (2.8,2.9,2.10,2.12) removed. The argument, u, is the set of $4(L+1)(1+2M)(1+2N)-(L+1)$ coefficients in the expansion of the velocity and pressure fields with the $(L+1)$ coefficients, $p_{l,0,0} \forall l \in \{0,..L\}$, removed since these pressure coefficients appear in no equations. The parameter, λ, is one of the set of parameters,

$$\{Re, \alpha_y, \alpha_z, V_0, \Omega, F_y, F_z, c_y, c_z\}.$$

2.3 Path Following

We use the methods of H. B. Keller to study the path,

$$\Gamma = \{(u(\lambda),\lambda) : F(u(\lambda),\lambda) = 0, \forall \lambda_a < \lambda < \lambda_b\}.$$

We use the following algorithm to find solutions along the path. The subscript, i, indexes solutions along the path.

Algorithm for Regular Path

Step 1 Start with an initial solution, (u_0, λ_0). Construct the Jacobian,

$$F_u^0 = \frac{\partial F(u_0; \lambda_0)}{\partial u}.$$

Step 2 Construct the initial iterate and initial parameter with one of the following:

- constant value continuation: $\lambda_i = \lambda_{i-1} + \delta\lambda, u_i^0 = u_{i-1}$
- or secant continuation: $\lambda_i = \lambda_{i-1} + \delta\lambda$,
  $u_i^0 = u_{i-1} + \frac{\lambda_i - \lambda_{i-1}}{\lambda_{i-1} - \lambda_{i-2}}(u_{i-1} - u_{i-2})$

Step 3 Compute the special Newton iterates (indexed by $\nu = 1, 2, ...$),

$$F_u^0 \epsilon^\nu = -F(u_i^\nu; \lambda_i),$$

$$u_i^{\nu+1} = u_i^\nu + \epsilon_i^\nu,$$

until $||\epsilon_i^N||_{l_1} < \epsilon$.

Step 4 Set $u_i = u_i^{N+1}$. If the parameter, λ_i, is still in the range we wish to study, and the number of iterations is small, e.g., $N < 30$, return to Step 2.

This algorithm may fail for several different reasons. One is that the step $\delta\lambda$ is too large. In this case, we decrease the step size. Another reason the algorithm may fail is that the Jacobian may need to be recomputed. Lastly, we could have stepped beyond a fold or crossed a bifurcation point. These last two failures require special algorithms to switch branches at a bifurcation point or step around a fold. We discuss these next.

2.3.1 Fold Points

Near a fold point, we find that we need to constantly decrease the step size and recompute the Jacobian in order to have the iterates in Step 3 converge. Furthermore, the condition number of the Jacobian increases rapidly. The work of Keller suggests that we change our continuation to some other parameter. We shall switch to continuation in the shear stress at the lower plate:

$$\bar{\tau}(\vec{V}) = -\frac{1}{\lambda_y \lambda_z} \int_0^{\lambda_y} \int_0^{\lambda_z} \frac{\partial v}{\partial x}(-1/2, y, z) dy dz. \tag{2.14}$$

In Taylor–Couette flow τ corresponds to the torque of the inner cylinder. Nagata (see [8]) introduces this parameter in his study of these flows. We adjoin the equation,

$$\tau(u) = \bar{\tau}(\vec{V}_a) = \tau_i \tag{2.15}$$

to $F(u;\lambda) = 0$. We study the solutions of the expanded system,

$$G(u(\tau_i), \lambda(\tau_i); \tau_i) = \begin{pmatrix} F(u(\tau_i), \lambda(\tau_i)) \\ \tau(u(\tau_i)) - \tau_i \end{pmatrix} = \begin{pmatrix} 0 \end{pmatrix}. \tag{2.16}$$

By varying τ_i we can study the path of solutions

$$\hat{\Gamma} = \{(u(\tau_i), \lambda(\tau_i), \tau_i) : F(u,\lambda) = 0, \tau(u) = \tau_i, \forall \tau_a < \tau_i < \tau_b\}.$$

This leads to a slightly different algorithm in which we solve for λ and we continue in the shear stress, τ_i. Again, the subscript, i, indexes solutions along the path.

Algorithm for Path at Fold

Step 1 Start with an initial solution, (u_0, λ_0). Construct the Jacobian,

$$G_x^0 = [G_u^0 : G_\lambda^0] = \begin{bmatrix} F_u^0 & F_\lambda^0 \\ \tau_u & 0 \end{bmatrix}.$$

Step 2 Construct the initial iterate and new parameter with one of the following:

- constant value continuation: $\tau_i = \tau_{i-1} + \delta\tau, u_i^0 = u_{i-1}, \lambda_i^0 = \lambda_{i-1}$
- or secant continuation:

$$\tau_i = \tau_{i-1} + \delta\tau,$$

$$u_i^0 = u_{i-1} + \frac{\tau_i - \tau_{i-1}}{\tau_{i-1} - \tau_{i-2}}(u_{i-1} - u_{i-2})$$

$$\lambda_i^0 = \lambda_{i-1} + \frac{\tau_i - \tau_{i-1}}{\tau_{i-1} - \tau_{i-2}}(\lambda_{i-1} - \lambda_{i-2})$$

Step 3 Compute the special Newton iterates (indexed by $\nu = 1, 2, ...$),

$$G_x^0 \begin{pmatrix} \epsilon_i^\nu \\ l_i^\nu \end{pmatrix} = \begin{pmatrix} -F(u_i^\nu; \lambda_i^\nu) \\ -\tau(u_i^\nu) + \tau_i \end{pmatrix},$$

$$u_i^{\nu+1} = u_i^\nu + \epsilon_i^\nu,$$

$$\lambda_i^{\nu+1} = \lambda_i^\nu + l_i^\nu,$$

until $||\epsilon_i^N||_{l_1} + |l_i^N| < \epsilon$.

Step 4 Set $u_i = u_i^{N+1}, \lambda_i = \lambda_i^{N+1}$. If $\tau_a < \tau_i < \tau_b$, is still in the range we wish to study, and the number of iterations, N, is small, return to Step 2.

For any given fold, we find we only need to compute the Jacobian, G_x^0, once. When the iterations in step 3 fail to converge, we return to continuation in λ.

2.3.2 Bifurcation Points

In the case of two intersecting paths, we have a bifurcation point. In this problem, we study two bifurcation points. One bifurcation point is an intersection of a solution depending only on x and a solution depending on x and z. We call the solution depending only upon x the Couette solution. We call the solution depending on x and z the vortex solution. The other bifurcation point is an intersection of a solution depending on all three domain variables and the vortex solution. The solution depending on all three variables is called a wavy vortex. See Figure 3.4 for a picture of these paths and their intersections.

Each of these bifurcation points presents a problem for the computation. In particular, we wish to locate the bifurcation points and to switch the path of solutions which we are following. In the generic case, we would expect the determinant of the Jacobian to change sign when crossing a bifurcation point. In both of the bifurcation cases above, the determinant of the Jacobian in step 1 of the algorithm for a regular path does not change sign since the null space of the Jacobian at the bifurcation point is two dimensional.

The bifurcation from the Couette solution to the vortex solution illustrates the difficulties of both bifurcations the most clearly. The Couette solution,

$$\vec{U}_C = \begin{pmatrix} 0 \\ -x \\ 0 \end{pmatrix},$$

$$p_C = \frac{\Omega x^2}{4},$$

is a solution for all (Re, Ω, α_z). At $(Re = 600, \Omega_c = 1.43, \alpha_z = 3.1163)$ the Jacobian in Step 1 of the regular path algorithm is singular. The null vectors are only a function of z. Since the Navier–Stokes equations are autonomous in z and the boundary conditions are periodic in z, the null vectors have a phase freedom. As a result, the Jacobian is singular with two zero eigenvalues. This means that the Jacobian does not change sign as Ω varies from below Ω_c to above Ω_c. This make detection of this bifurcation difficult.

In order to accurately locate the bifurcation point we make an ad–hoc substitution of the phase constraint,

$$\Phi_z(u) = \bar{\Phi}_z(\vec{V}_a) = \int_{-\frac{1}{2}}^{\frac{1}{2}} \frac{dx}{\sqrt{1-4x^2}} \int_0^{\lambda_y} dy \int_0^{\lambda_z} dz \sin(2\pi y/\lambda_y) w_a(x,y,z) = 0, \tag{2.17}$$

for the corresponding momentum constraint,

$$\langle C_{0,0,1}, - \text{ Re } (\vec{V}_a \cdot \vec{\nabla}) w_a + \nabla^2 w_a - \vec{\nabla} p_a + c_y \partial_y w_a + c_z \partial_z w_a \rangle = 0,$$

in the equations, $F(u;\lambda) = 0$. The determinant of the Jacobian of this new system changes sign at the bifurcation point. We use a secant method to find the zero of the determinant. This is the first step in our algorithm to switch paths from the Couette solution to the vortex solution.

Algorithm to Switch Paths from Couette to Vortex Solutions

Step 1. Accurately find the parameter value λ^* at which

$$F_u^* = \frac{\partial F(u(\lambda^*), \lambda^*)}{\partial u}$$

is singular.

Step 2. Find the right nullvector, ϕ, of the singular Jacobian with $\Phi_z(\phi) = 0$.

Step 3. Find a left nullvector, ψ, of the singular Jacobian with $\Phi_z(\psi) = 0$.

Step 4. Construct the initial guess for a solution on the new branch, $u_i^o = u(\lambda^*) + \epsilon\phi$.

Step 5. Compute the Newton iterates on the inflated system,

$$\begin{pmatrix} F(u, \lambda, c_z) \\ \psi \cdot u \\ \Phi_z(u) \end{pmatrix} = \begin{pmatrix} 0 \\ \psi \cdot u_i^0 \\ 0 \end{pmatrix}$$

We add the phase constraint in step 5 in order to make the solution on the new branch unique. Without the phase constraint, the solution has a phase freedom. This freedom is a result of the periodic boundary conditions and the fact that the Navier–Stokes equations are autonomous in z. Since we now have one more equation, we now solve for the wave speed, c_z, in addition to the other variables. In our calculations, we chose the parameter, λ, to be the rotation, Ω. After the Newton iterates have converged, we find that using shear stress continuation in the Algorithm for the Path at a Fold works best for the extension of the path from the bifurcation point.

A completely analogous algorithm is used to switch from the vortex solution path to the wavy vortex path. Once again, in order to accurately locate the bifurcation point we make an ad–hoc substitution of the phase constraint,

$$\Phi_y(u) = \bar{\Phi}_y(\vec{V}_a) = \int_{-\frac{1}{2}}^{\frac{1}{2}} \frac{dx}{\sqrt{1-4x^2}} \int_0^{\lambda_y} dy \int_0^{\lambda_z} dz \cos(2\pi z/\lambda_z) u_a(x, y, z) = 0, \tag{2.18}$$

for the momentum constraint,

$$\langle S_{0,1,0}, - \text{ Re } (\vec{V}_a \cdot \vec{\nabla})u_a + \nabla^2 u_a - \vec{\nabla} p_a - 2\Omega v_a + c_y \partial_y u_a + c_z \partial_z u_a \rangle = 0,$$

appearing in the expanded system,

$$H(u, \lambda, c_z) = \begin{pmatrix} F(u, c_z, \lambda) \\ \Phi_z(u) \end{pmatrix}.$$

This is the first step in the Algorithm to Switch Paths from Vortex to Wavy Vortex Solutions

Algorithm to Switch Paths from Vortex to Wavy Vortex Solutions

Step 1. Accurately find the parameter value λ^* at which the Jacobian,

$$(H_u(u(\lambda^*), \lambda^*, c_z) | H_{c_z}(u(\lambda^*), \lambda^*, c_z)),$$

is singular.

Step 2. Find the right nullvector, ϕ, of the singular Jacobian with $\Phi_y(\phi) = 0$.

Step 3. Find a left nullvector, ψ, of the singular Jacobian with $\Phi_y(\psi) = 0$.

Step 4. Construct the initial guess for a solution on the new branch, $u_i^o = u(\lambda^*) + \epsilon\phi$.

Step 5. Compute the Newton iterates on the inflated system,

$$\begin{pmatrix} F(u, \lambda, c_y, c_z) \\ \psi \cdot u \\ \Phi_z(u) \\ \Phi_y(u) \end{pmatrix} = \begin{pmatrix} 0 \\ \psi \cdot u_i^0 \\ 0 \\ 0 \end{pmatrix}$$

It would have been more reasonable to use the condition $\phi \cdot u = \phi \cdot u_i^0$ rather that the condition $\psi \cdot u = \psi \cdot u_i^0$; however, we did not.

2.4 Implementation

We have left several points of our method vague and we try to clarify them here. In particular, we will discuss how we compute the inner products in Eqs. (2.4)–(2.5), we will discuss the construction of the Jacobians and we will discuss the computation of the null vectors.

2.4.1 Inner Products and the Jacobians

The velocity and pressure fields are approximated by truncated series of Chebyshev polynomials and Fourier series of the form,

$$q_a(x,y,z) = \sum_{l=0}^{L} \sum_{m=-M}^{M} \sum_{n=-N}^{N} q_{l,m,n} A_{l,m,n}(x,y,z),$$

where q is one of u, v, w, or p. The basis functions, $A_{l,m,n}$, are given in Section 2.2. Each of the derivatives in Eqs. (2.4)–(2.5) are recast so that the inner products are analytically calculated. We use the well–known derivatives of the Fourier series,

$$\partial_y q_a(x,y,z) = \sum_{l=0}^{L} \sum_{m=-M}^{M} \sum_{n=-N}^{N} (im\alpha_y) q_{l,m,n} A_{l,m,n}(x,y,z).$$

The analogous derivative in the z direction is also used. For the derivatives in the x direction, we use the expansions computed by Gottlieb and Orszag [3]. This only leaves this issue of the multiplications of fields appearing in the

convective terms, $(\vec{V}_a \cdot \vec{\nabla})\vec{V}_a$, of Eq. (2.4). Since we use relatively few Fourier and Chebyshev modes in our truncated series expansion of the velocity and pressure fields, we compute the multiplications by convolutions rather than by collocation methods. The advantage of the convolutions is that we can analytically compute the derivatives of each of the inner products in Eqs. (2.4)–(2.5) with respect to the coefficients in the expansions of the velocity and pressure fields.

2.4.2 The Null Vectors

Since the Jacobian is nearly singular at the points where we wish to compute approximate null vectors, we use inverse iterations to find both the right and left null spaces. This is easily done since LINPACK provides routines for solving the problems,

$$A\phi_{i+1} = \phi_i/||\phi_i|| - \Phi_y(\phi_i/||\phi_i||) - \Phi_z(\phi_i/||\phi_i||),$$

$$A^T\psi_{i+1} = \psi_i/||\psi_i|| - \Phi_y(\psi_i/||\psi_i||) - \Phi_z(\psi_i/||\psi_i||),$$

$$i = 0, 1, 2, ...N.$$

To start the iterations, we chose a random initial vector ϕ_0 or ψ_0. After N ($\doteq 30$) iterations, the norm, $||\phi_i||$ or $||\psi_i||$, converges. We use $\phi_N/||\phi_N||$ as the null vector of the Jacobian. Similarly, we use $\psi_N/||\psi_N||$ as the left null vector of the Jacobian.

2.4.3 Symmetry and Optimization

In the special case of no forcing ($\vec{F} = 0$), we find solutions of (2.13) which have a symmetry which allows us to eliminate half the variables and equations. All the real parts of the coefficients of the velocity components are zero whenever their indices sum to a multiple of two. Similarly, the imaginary parts of the velocity coefficients with odd summed indices are zero.

$$\left.\begin{array}{c} \text{Imaginary}(\vec{V}_{l,m,n}) = 0 \\ \text{Real}(p_{l,m,n}) = 0 \end{array}\right\} \forall (l+m+n)(\text{mod}2) = 1, \tag{2.19}$$

$$\left.\begin{array}{c} \text{Real}(\vec{V}_{l,m,n}) = 0 \\ \text{Imaginary}(p_{l,m,n}) = 0 \end{array}\right\} \forall (l+m+n)(\text{mod}2) = 0. \tag{2.20}$$

The wave speeds, $c_y = c_z = 0$, are also zero.

Solutions of this type can be obtained by performing Newton iterations on only half of the equations. In particular we perform Newton iterations on the equations,

$$0 = H(u;\lambda) = \begin{cases} \langle C_{l,m,n}, \vec{M}(\vec{V}_a, p_a)\rangle & \forall (l+m+n)(\text{mod}2) = 0 \\ \langle S_{l,m,n}, \vec{M}(\vec{V}_a, p_a)\rangle & \forall (l+m+n)(\text{mod}2) = 1 \\ \langle C_{l,m,n}, \vec{\nabla}\cdot\vec{V}_a\rangle & \forall (l+m+n)(\text{mod}2) = 1 \\ \langle S_{l,m,n}, \vec{\nabla}\cdot\vec{V}_a\rangle & \forall (l+m+n)(\text{mod}2) = 0 \\ \text{Boundary Conditions} & \end{cases} \tag{2.21}$$

$$\vec{M}(\vec{V}_a, p_a) = -\text{ Re }(\vec{V}_a\cdot\vec{\nabla})\vec{V}_a + \nabla^2\vec{V}_a - \vec{\nabla}p_a + 2\Omega(\hat{z}\times\vec{V}_a).$$

We solve for the coefficients not required to be zero by Eqs. (2.19) and (2.20). The boundary conditions we use for this half–size system are those not identically satisfied when the coefficients have the symmetry of Eqs. (2.19)

and (2.20). We only perform Newton iterates to solve for the coefficients which are not identically zero by Eqs. (2.19) and (2.20).

By only solving half the equations for half the variables, we save much memory and time. Every u satisfying $H(u, \lambda) = 0$ and Eqs. (2.19) and (2.20) was found to satisfy $F(u, \lambda)$.

Chapter 3

Results in Plane Shear Flow

In the case of shearing plates with no external forcing, we search for solutions of the equations,

$$0 = -\,\mathrm{Re}\,(\vec{V}\cdot\vec{\nabla})\vec{V} + \nabla^2\vec{V} - \vec{\nabla}p + 2\Omega(\hat{z}\times\vec{V}), \tag{3.1}$$

$$0 = \vec{\nabla}\cdot\vec{V}, \tag{3.2}$$

with boundary conditions (1.11–1.16), $V_0 = 1$, and the two phase constraints, $\Phi_z(\vec{V}) = 0$ and $\Phi_y(\vec{V}) = 0$ defined in (2.17) and (2.18). We approximate the solutions to these equations using the methods described in Chapter 2. We are particularly interested in solutions with $\Omega = 0$.

3.1 Bifurcations and Solution Paths

3.1.1 From Couette Flow to Vortices

Couette flow,

$$\vec{V}_C = \begin{pmatrix} 0 \\ -x \\ 0 \end{pmatrix},$$

$$p_C = \frac{\Omega x^2}{4},$$

is a solution of Eqs. (3.1–3.2) for all (Re, Ω). The average (over the y and z directions for one period in each direction) of the y component of Couette flow is shown in Figure 3.1.

At certain values of (Re, α_z, Ω) we find a bifurcation from Couette flow. We know from the analysis in Appendix B that the locations of the bifurcations from the Couette solutions are a function of the Taylor number,

$$T = 2\Omega(Re - 2\Omega),$$

and the wave number, α_z. The locations of these bifurcation points are not independent functions of the Reynolds number and Ω. We call the Taylor number at which the Jacobian is singular the critical Taylor number (T_c).

Note that the Taylor number is quadratic in Ω. This means that for large enough Reynolds number,

$$Re > 2\sqrt{T_c},$$

there are at least two singular points. In the generic case, there are an even number of singular points. We will concentrate on the singular point with

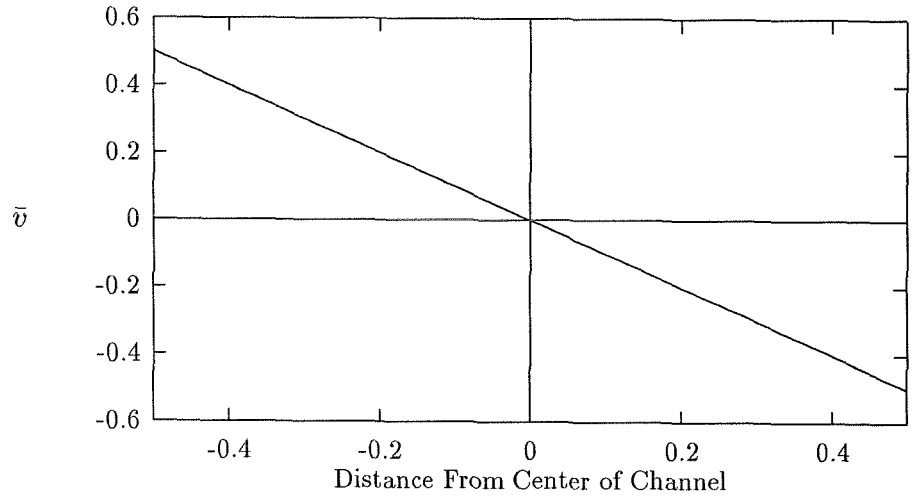

Figure 3.1: The y velocity as a function of distance from the center of the channel for Couette flow.

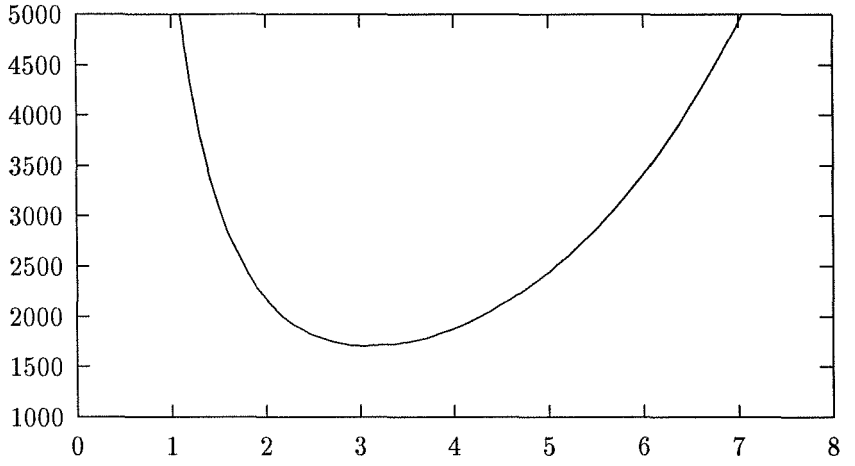

Figure 3.2: T_c vs α_z.

lowest critical Taylor number and $\Omega < Re/4$.

T_c varies with $\alpha_z = 2\pi/\lambda_z$; however, it does not vary with α_y. See Figure 3.2 for a graph of T_c as a function of α_z. Since the boundary conditions are periodic, if the Jacobian is singular at (T_c, λ_z) then the Jacobian is also singular for all periodicities which are integral multiples of $\lambda_{z,c}$, namely, $(T_c, n\lambda_z)$. Figure 3.3 is a graph of the critical Taylor number against the periodicity λ_z. Only the first 6 multiples of the fundamental mode are shown.

We compute these values of the critical Taylor number by fixing the Reynolds number at $Re = 600$. At different values of the wave number, α_z, we increase Ω from zero (in steps of .05). When the determinant of the Jacobian changes sign, we use a secant method to determine the value of Ω

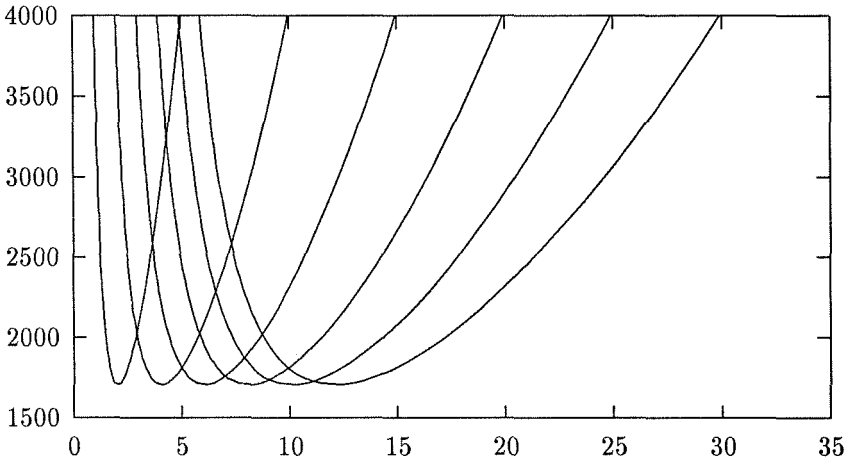

Figure 3.3: T_c vs λ_z when the x-direction is spanned by 33 Chebyshev polynomials.

at which the Jacobian has the smallest determinant. (We find that Ω can be determined to 14 digits by this secant method; although, the actual accuracy of this value of Ω could be affected by roundoff error or resolution of the solution space.) We then compute the Taylor number using $T = 2\Omega(Re - 2\Omega)$. We compute the Taylor number for different values of the wave number α_z. This gives us $T(\alpha_z)$. We then compute Newton iterations on the minimum problem,

$$\frac{\partial T}{\partial \alpha_z} = 0,$$

to find the minimum Taylor number. The results of this calculation are shown in Table 3.1 for several different resolutions of the solution. The minimum critical Taylor number is

$$T_c = 1707.76177710472$$

when the wave number is

$$\alpha_z = 3.116323555/n.$$

Table 3.1 shows that very few Chebyshev polynomials are necessary to accurately compute T_c. Couette flow only varies with x. As a result all the y and z modes decouple. Thus, the accuracy of the critical Taylor number does not depend upon the number of fourier modes in the y and z directions.

At the bifurcation point ($Re = 600, \alpha_z = 3.0, \Omega = 1.43$) we switch to the new branch of solutions (the vortex branch) by the methods discussed in Section 2. The Couette solution has a constant shear stress of 1.0 for all values of Ω. In contrast, the new branch of solutions (labeled 'vortex' in Figure 3.4) increases in shear stress with increasing Ω.

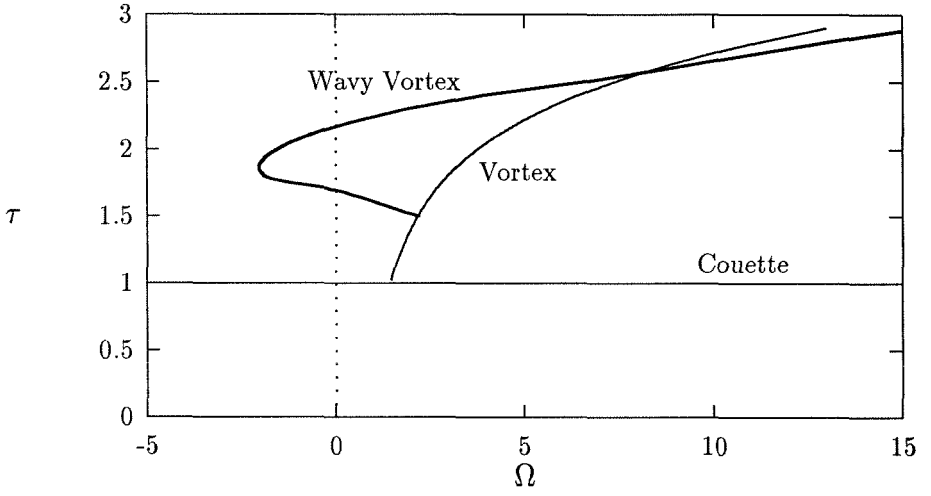

Figure 3.4: Shear Stress as a function of Ω. $Re = 600, \alpha_y = 1.6, \alpha_z = 3.0$. The lower intersection of vortex and wavy vortex branches is a bifurcation. The upper intersection of the vortex and wavy vortex branches is only graphical. (The flows are not the same at this point.) There are two wavy vortex solutions $\Omega = 0$. The solution with large shear stress is called the upper branch solution and the low shear stress is called the lower branch solution. The resolution is $(L, M, N) = (14, 3, 3)$ in this picture.

minimizing α_z	minimum T_c	L
3.1163235547	1707.761777104727	16
3.1163235550	1707.761777104721	18
3.1163235549	1707.761777104720	20
3.1163235548	1707.761777104720	24
3.1163235548	1707.761777104719	30

Table 3.1: Only 16 Chebyshev polynomials are needed to resolve the critical Taylor number (T_c) to 15 digits of accuracy. L is the number of Chebyshev polynomials used.

These vortices have some symmetries. The null vector at the bifurcation point has components only in the direction of the first harmonic of the fundamental wavelength in the z-direction. The solution branch only varies with x and z. There is no y variation. We graph the mean flow in the y direction in Figure 3.5 and the flow perpendicular to y in Figure 3.6. We can write the vortex solution in the simpler form,

$$\vec{V}_a = \sum_{l=0}^{L} \sum_{n=-N}^{N} \vec{V}_{l0n} T_l(2x) e^{i(n\alpha_z z)},$$

$$p_a = \sum_{l=0}^{L} \sum_{n=-N}^{N} p_{l0n} T_l(2x) e^{i(n\alpha_z z)}.$$

We follow the vortex solution from $\Omega = 1.43$ where it bifurcates from Couette flow to $\Omega = 13$. During this continuation the determinant of the Jacobian changes sign at $\Omega = 2.1725$ signalling a secondary bifurcation. We discuss the new branch of solutions bifurcating from the vortex branch in

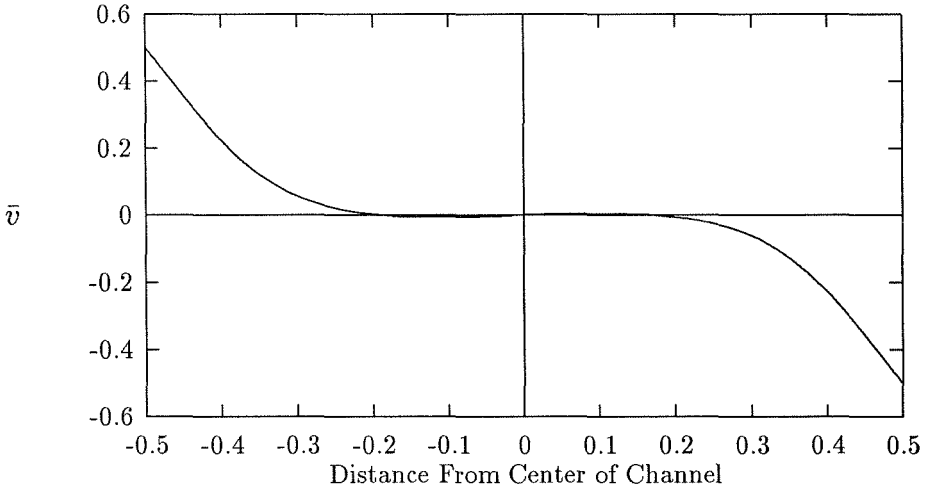

Figure 3.5: The mean (over a period in y and z) of the flow in the y direction for the vortex solution at Re=600, $\Omega = 13$, $\alpha_z = 3.0$.

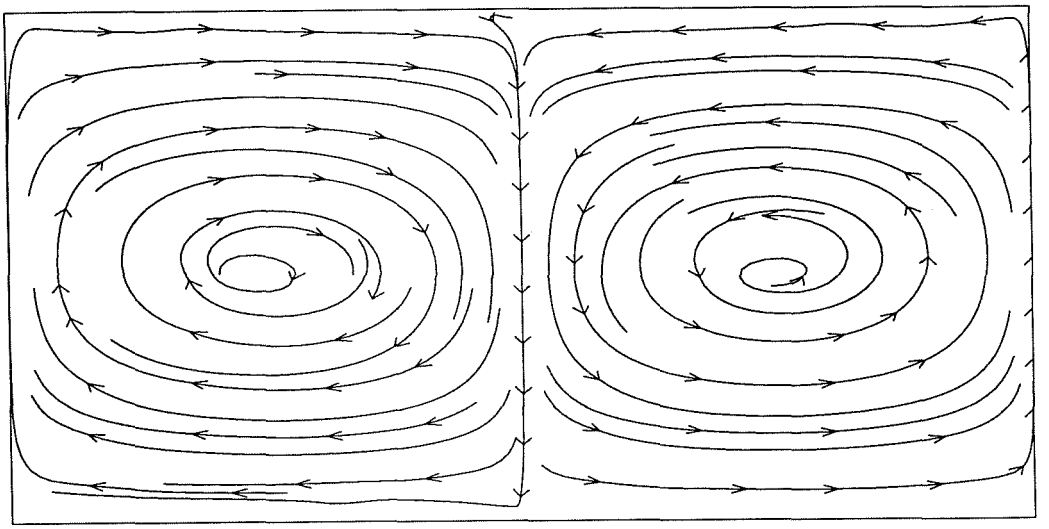

Figure 3.6: The velocity field in the xz plane for the vortex solution at Re=600, $\Omega = 13$, $\alpha_z = 3.0$. The lower plate is shearing out of the paper on the lower edge of the image.

Section 3.1.2. The new branch of solutions is labeled "Wavy Vortex" in Figure 3.4.

At lower Reynolds numbers (i.e., $Re < 250$), we have sufficient resolution to compute the the full path of vortex solutions. At wave number, $\alpha_z = 3.0$, we have a critical Taylor number, $T_c = 1711.28$. Thus, at Reynolds number 85.0, the two values of Ω which satisfy the equation,

$$T_c = 2\Omega(Re - 2\Omega),$$

are ($\Omega = 16.377$ and $\Omega = 26.123$). As can be seen in Figure 3.7, there is one vortex solution branch which intersects the Couette flow branch at these two points.

We have discussed the bifurcations from Couette flow with low critical Taylor numbers ($T_{c,1} < 2000$). At the same wave number, $\alpha_z = 3.0$, there are a sequence of critical Taylor numbers, say, $T_{c,\nu}, \nu = 1, 2, \ldots$. The $T_{c,\nu}$ are the sequence of eigenvalues of the problem B.6 in Appendix B. While we did not accurately locate them, the next two values of the critical Taylor number are $T_{c,2} \doteq 26,100$ and $T_{c,3} \doteq 182,300$. These critical Taylor numbers also vary with α_z. In Figure 3.8 we show the relation between $T_{c,2}$ and the wave number, α_z. Note that the minimum value of $T_{c,2}$ is nearly ten times the minimum value of $T_{c,1}$ (graphed in Figure 3.2 and labeled T_c.)

3.1.2 From Vortices to Wavy Vortices

On the vortex solution branch bifurcating from Couette flow the Jacobian is singular at parameter values $Re = 600, \Omega = 2.17, \alpha_y = 1.6, \alpha_z = 3.0$. We switch paths using the algorithm described in Section 2. The new path of

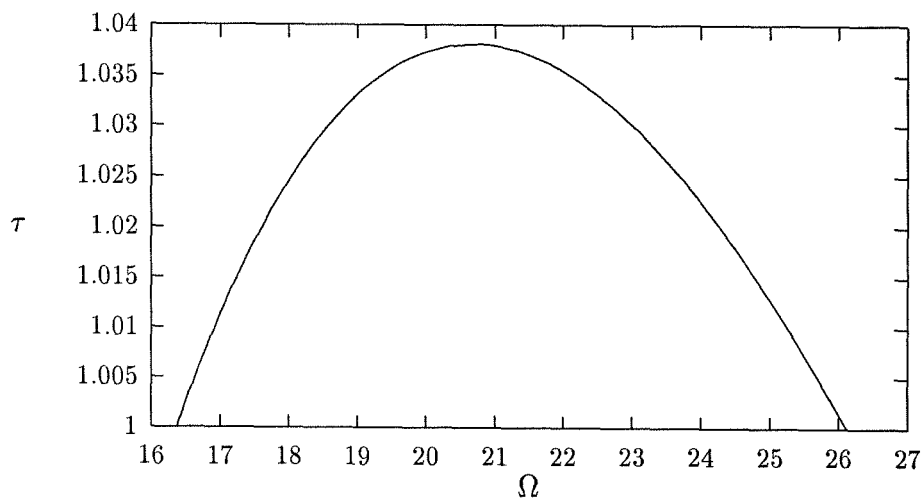

Figure 3.7: Shear Stress vs. Ω at $Re = 85.0, \alpha_z = 3.0, \alpha_y = 1.6$. This branch of vortices shows that the two values of Ω satisfying $2\Omega(Re - 2\Omega) = T_c$ correspond to bifurcation points on the same branch of vortex solutions.

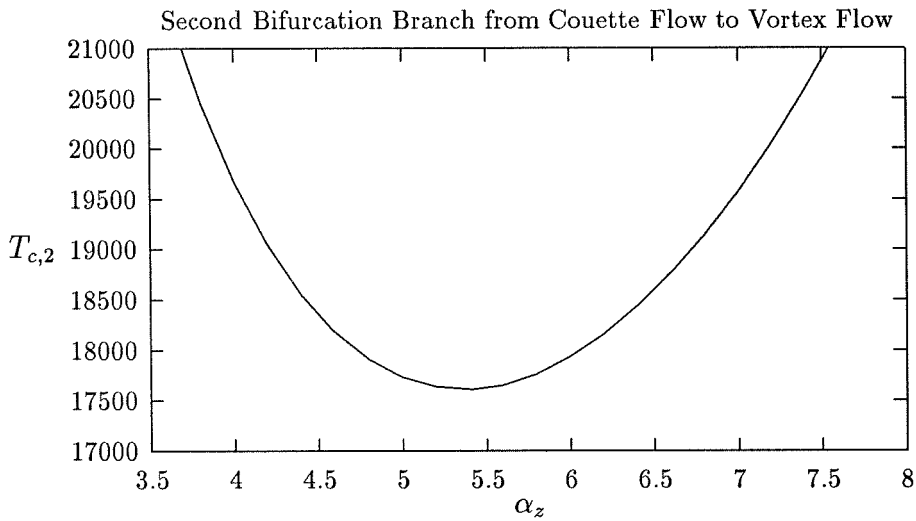

Figure 3.8: Couette flow bifurcates to a different path of solutions at higher Taylor number. This second branch of critical Taylor numbers has a minimum near 17700 when α_z is near 5.4.

solutions is labeled 'Wavy Vortex' in Figure 3.4. Note that it has a fold point and two solutions at $\Omega = 0$.

We study these three solutions on this path. We study the solution at the fold point, ($\tau = 1.86, \Omega = -2.07$.) We also study the solutions at $\Omega = 0$. We call the solution (at $\Omega = 0$) with larger shear stress the upper branch solution and the solution with smaller shear stress the lower branch solution.

Table 3.2, indicates that there is a relative error of less than 4% in the shear stress for resolutions above $(L, M, N) = (13, 3, 3)$. We use the resolution (14,3,3) for the rest of the computations discussed in this chapter.

In Figure 3.9 we show the mean velocity in the y-direction for comparison with the vortex and Couette solutions (Figures 3.5 and 3.1 respectively.) In Figure 3.10 we graph x-z cross sections of the velocity field for different values of y. Compare with the vortex solution in Figure 3.6.

While the solutions (at $\Omega = 0$), are well approximated, we do not yet know anything about their stability. We also do not know the minimum value of the Reynolds number at which these solutions exist.

3.2 Minimum Reynolds Number Solutions

As we have seen (in Figure 3.4), there are the upper branch and lower branch wavy vortex solutions at $\Omega = 0$. These solutions vary with Reynolds

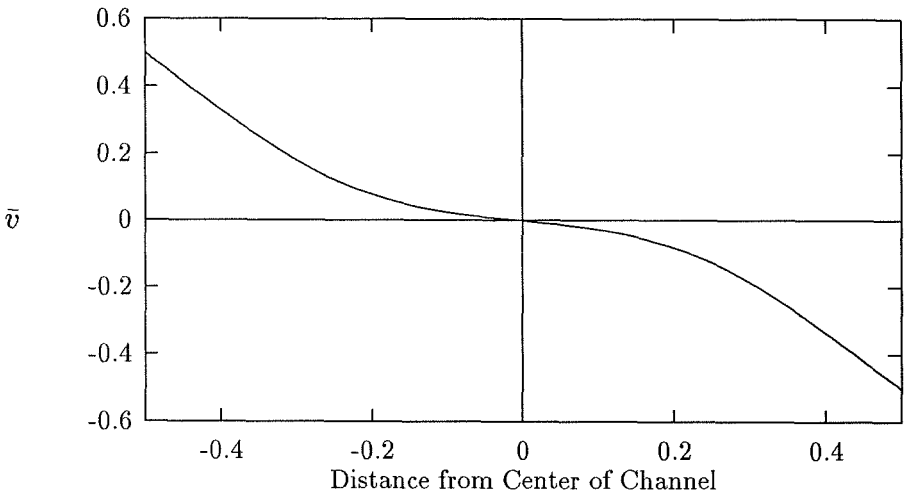

Figure 3.9: The mean flow in the y direction of the lower branch solution as a function of distance from center of channel. $Re = 600, \alpha_y = 1.6, \alpha_z = 3.0, \Omega = 0, \tau = 1.7$.

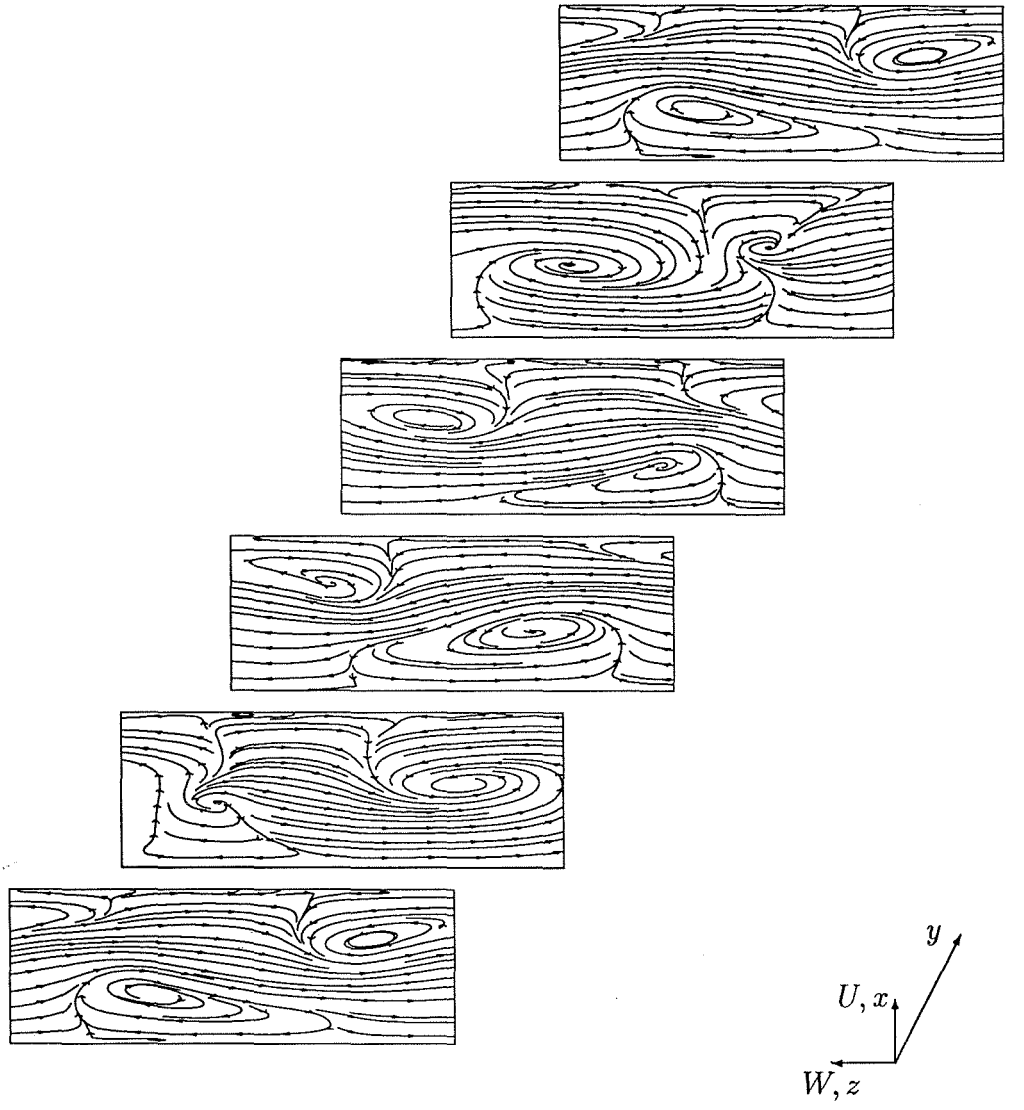

Figure 3.10: Cross sections (at $y = 0, \frac{2\pi}{5}, \frac{4\pi}{5}, \frac{6\pi}{5}, \frac{8\pi}{5}, 2\pi$) of the velocity field of the lower branch wavy vortex solution in the xz plane. The left-bottom cross section is at $y = 0$ and the upper-right cross section is at $y = 2\pi$. $Re = 600, \alpha_y = 1.6, \alpha_z = 3.0$. The lower plate is shearing out of the paper at the bottom of each cross section.

resolution L,M,N	shear stress at lower plate
13,3,3	1.72177413
14,3,3	1.69405548
15,3,3	1.70084151
16,3,3	1.69987208
17,3,3	1.69936109
18,3,3	1.69959818
14,3,4	1.68283399
14,3,5	1.66029900
14,4,4	1.66777241
14,4,5	1.67317174

Table 3.2: The lower branch wavy vortex solution (at $\Omega = 0$) is resolved well enough that the shear stress of the solution at the lower plate has a relative error of less than 4%.

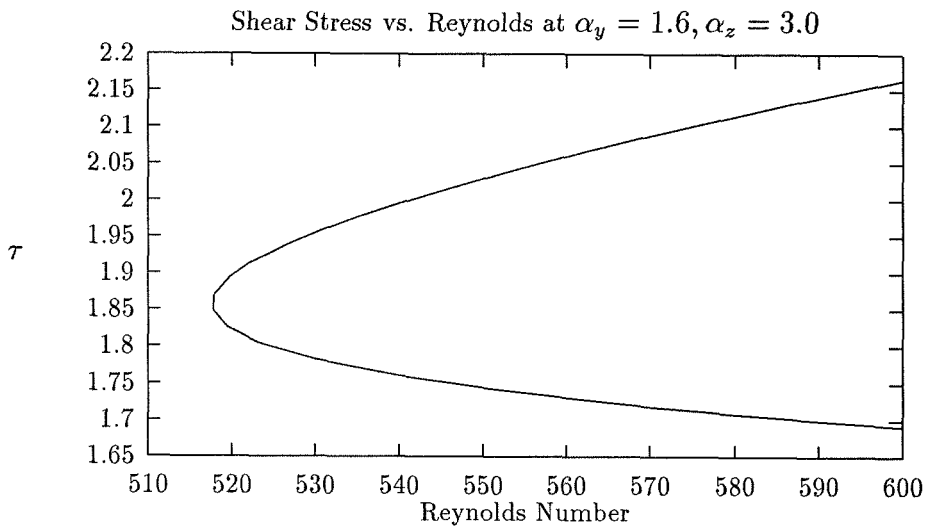

Figure 3.11: As the Reynolds number decreases from 600.0, the upper and lower branches of the $\Omega = 0$ wavy vortices coalesce and disappear.

number, shear stress, and the two wave numbers. We study the problem,

$$\begin{pmatrix} F(u(\tau_0, \alpha_y, \alpha_z), Re(\tau_0, \alpha_y, \alpha_z)) \\ \Omega \\ \tau(u) - \tau_0 \end{pmatrix} = 0, \tag{3.3}$$

to elucidate this variation.

We start with the lower branch solution and increase the shear stress (τ_0). We find (for $\alpha_y = 1.6, \alpha_z = 3.0$) that the Reynolds number decreases, reaches a minimum and increases again. Figure 3.11 shows this variation of Reynolds number with shear stress. This path includes the upper branch solution. For these values of the wave numbers, the minimum Reynolds number is 520; however, we find lower Reynolds number flows by varying the wave numbers.

In order to find the minimum Reynolds number for all (local) wavenumbers and shear stresses, we solve the minimum problem,

$$\begin{pmatrix} \frac{\partial Re}{\partial \tau} \\ \frac{\partial Re}{\partial \alpha_y} \\ \frac{\partial Re}{\partial \alpha_z} \end{pmatrix} = 0 \tag{3.4}$$

by Newton's method. We start the Newton iterations with the solution at $\tau = 1.85, \alpha_y = 1.6, \alpha_z = 3.0$ in Figure 3.11. Each step of Newton's method requires 42 solutions of the Navier–Stokes equations in order to evaluate the finite difference approximations of the derivatives appearing in the Newton iterations for this minimum problem. We find the minimum at the following values of the parameters:

$$Re = 467.3,$$

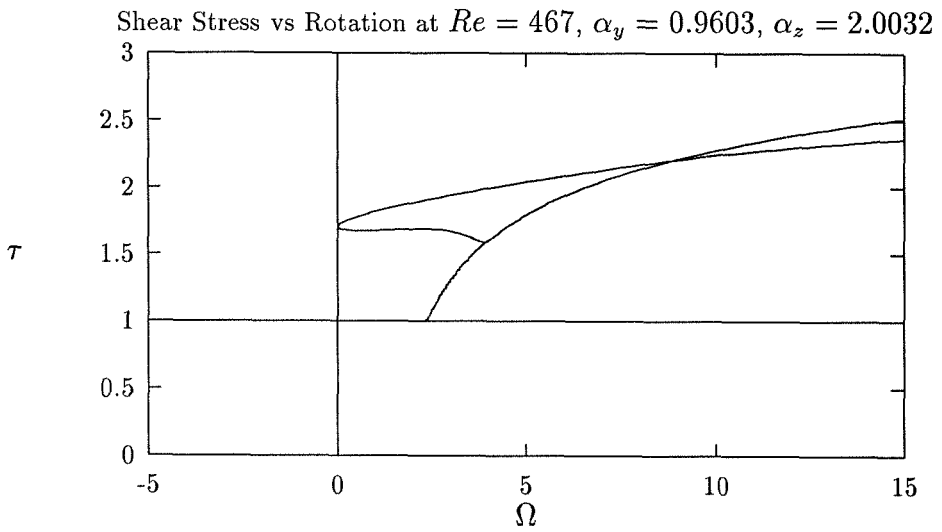

Figure 3.12: Solution path with resolution (L,M,N)=(14,3,3) at minimum Reynolds number Re=467. $\alpha_y = .96$, $\alpha_z = 2.0$.

$$\tau = 1.70,$$

$$\alpha_y = 0.96,$$

$$\alpha_z = 2.00.$$

These values are calculated with a resolution of $(L, M, N) = (14, 3, 3)$. We trace the solution path (τ vs Ω) for these values of the Reynolds number and wave numbers in Figure 3.12.

3.3 Linear Stability

While we are fairly certain that we have approximated solutions of the time independent Navier–Stokes equations, we need to know if these solutions are stable solutions of the time dependent equations,

$$\frac{\partial V}{\partial t} = -\text{Re}\,(\vec{V}\cdot\vec{\nabla})\vec{V} + \nabla^2\vec{V} - \vec{\nabla}p + 2\Omega(\hat{z}\times\vec{V}), \tag{3.5}$$

$$0 = \vec{\nabla}\cdot\vec{V}. \tag{3.6}$$

The time has been scaled by the square of the channel width and viscosity. We perform the usual stability analysis. We look for non-zero eigenvectors , $\vec{\epsilon}, \rho$, satisfying the following equations:

$$\lambda\vec{\epsilon} = -\text{Re}\,[(\vec{V}_a\cdot\vec{\nabla})\vec{\epsilon} + (\vec{\epsilon}\cdot\vec{\nabla})\vec{V}_a] + \nabla^2\vec{\epsilon} - \vec{\nabla}\rho + 2\Omega(\hat{z}\times\vec{\epsilon}) \tag{3.7}$$

$$0 = \vec{\nabla}\cdot\vec{\epsilon}. \tag{3.8}$$

We require $\vec{\epsilon}$ to satisfy the symmetry discussed in Section 2.4.3. We approximate $\vec{\epsilon}$ and ρ in the same way as $\vec{V}_a$ and p_a. $\vec{\epsilon}$ is subject to Dirichlet boundary conditions at the x boundaries and periodic boundary conditions in y and z. In this way we get a (singular) generalized eigenvalue problem of order 1454 (for $(L, M, N) = (14, 3, 3)$). We know from theory that there are some eigenvalues at infinity for (singular) generalized eigenvalue problems; however, our numerical analysis (in finite precision) perturb the eigenvalues at infinity to large magnitude eigenvalues. In particular if we use D Galerkin projections of Eq. 3.7 and E projections of Eq. 3.8, then there are $D - E$ eigenvalues. In our particular case, we have 968 projections of Eq. 3.7 and 360 projections of Eq. 3.8. Thus, we should have 588 meaningful eigenvalues

and many large magnitude eigenvalues. Note that unstable eigenvalues have Real(λ) $>$ 0 and stable eigenvalues have Real(λ) $<$ 0. We compute these eigenvalues using EISPACK.

First we study the stability of the lower branch solution. The parameters are $Re = 600, \alpha_y = 1.6, \alpha_z = 3.0, \Omega = 0$, and $\tau = 1.694$. Figure 3.13 shows the scattered eigenvalues of large magnitude. We look at the center of this figure scaled by 100 in Figure 3.14. Note the cluster of 588 eigenvalues near the origin. This cluster of eigenvalues is shown at much larger scale in Figure 3.15. The cluster of eigenvalues along the imaginary axis is scaled again in Figure 3.16. Lastly, we show the eigenvalues near the origin in Figure 3.17. Note that there is one eigenvalue in the right half plane. This means that the solution is unstable.

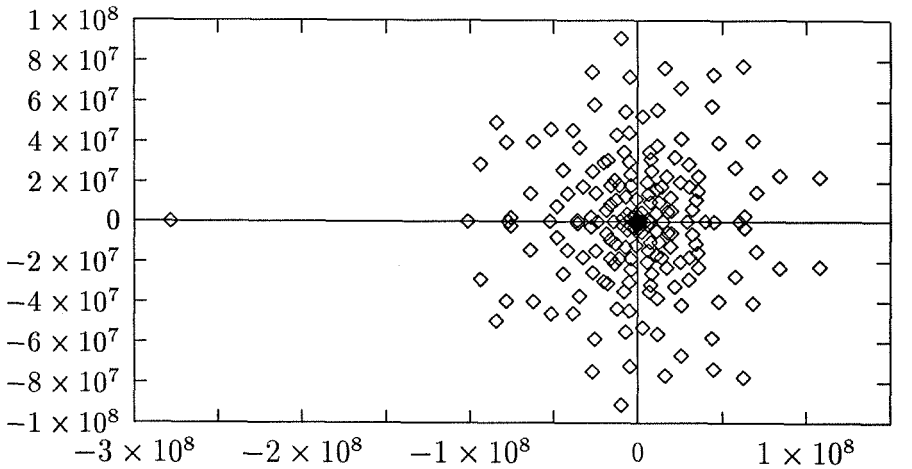

Figure 3.13: All the eigenvalues that we compute (including those perturbed from infinity) of the lower branch wavy vortex solution. We magnify the center of this graph by a factor of 100 to get the next figure.

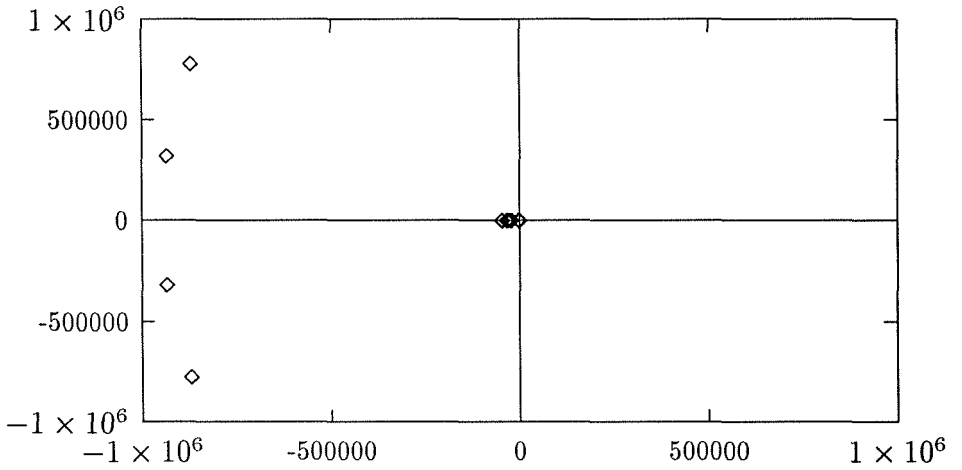

Figure 3.14: The eigenvalues near the origin of the previous figure. There are 588 eigenvalues clustered near the origin. This cluster of eigenvalues is shown (magnified) in the next figure.

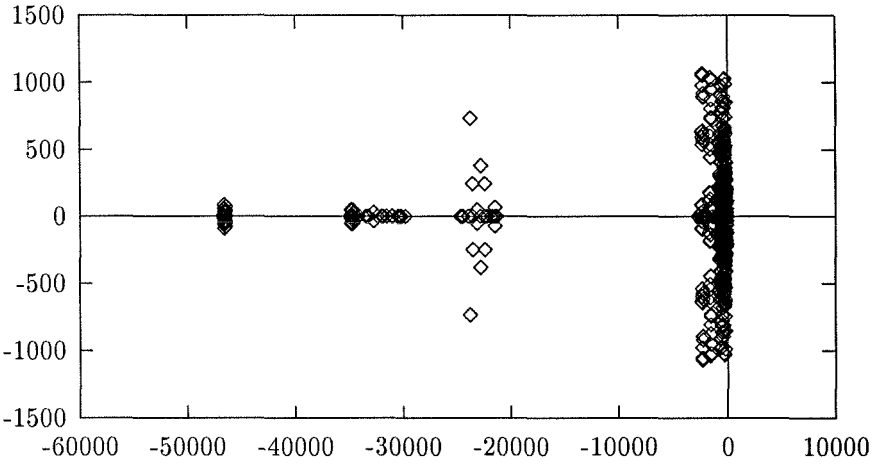

Figure 3.15: The 588 meaningful eigenvalues of the problem. The eigenvalues along the imaginary axis are magnified in the next figure.

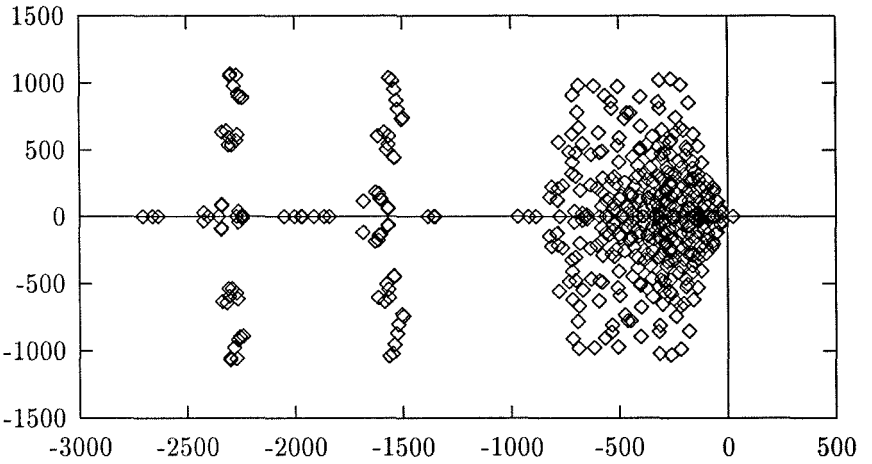

Figure 3.16: The eigenvalues near the imaginary axis.

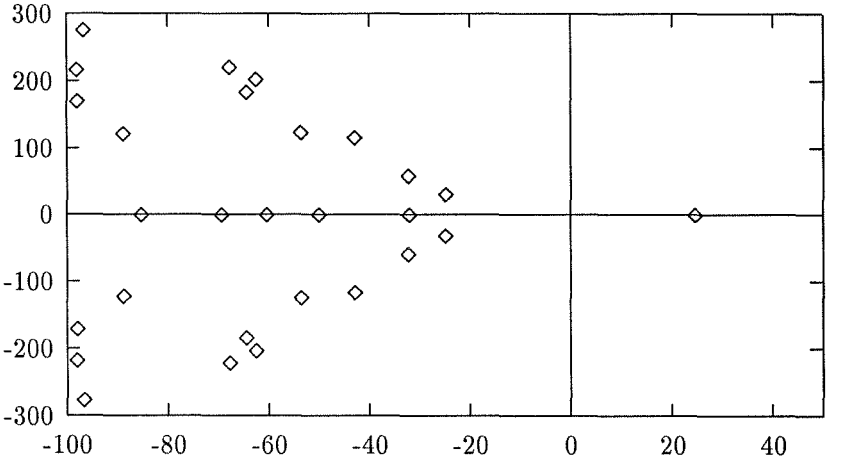

Figure 3.17: Eigenvalues of lower branch solution near the origin. Note the one unstable eigenvalue to the right of the imaginary axis. The parameter values are $Re = 600, \alpha_y = 1.6, \alpha_z = 3.0, \tau = 1.7$.

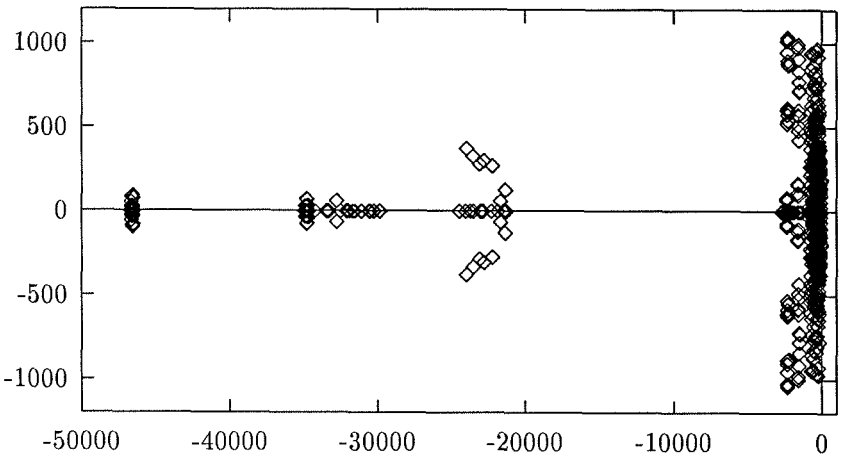

Figure 3.18: The eigenvalues from the linear stability analysis of the solution at the fold point for the wavy vortex solution at $Re = 600, \alpha_y = 1.6, \alpha_z = 3.0$. The cluster of 588 eigenvalues near the origin are shown here.

In Figure 3.4 we see that there is a fold in the graph of shear stress versus Ω. We study the linear stability of the wavy vortex solution at this fold. We plot the 588 meaningful eigenvalues in Figure 3.18. Once again we look at the eigenvalues near the origin (in Figure 3.19) and find that there is one neutrally stable eigenvalue.

Figures 3.20 and 3.21 show the eigenvalues of the upper branch solution. Note the pair of unstable eigenvalues in Figure 3.21.

Lastly, we study the stability at the minimum Reynolds number solution. These eigenvalues are plotted in Figures 3.22 and 3.23. Note the two eigen-

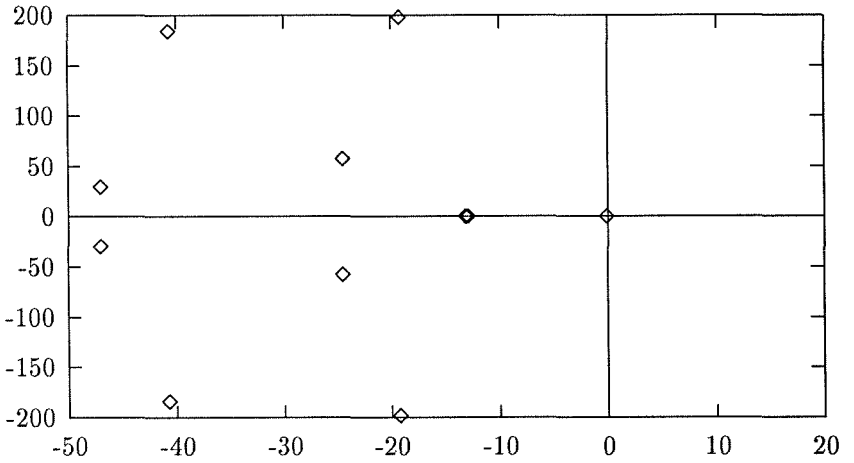

Figure 3.19: This figure shows the eigenvalues nearest the origin in the previous figure. The stability at the fold is neutral with only one neutrally stable eigenvalue and no unstable eigenvalues.

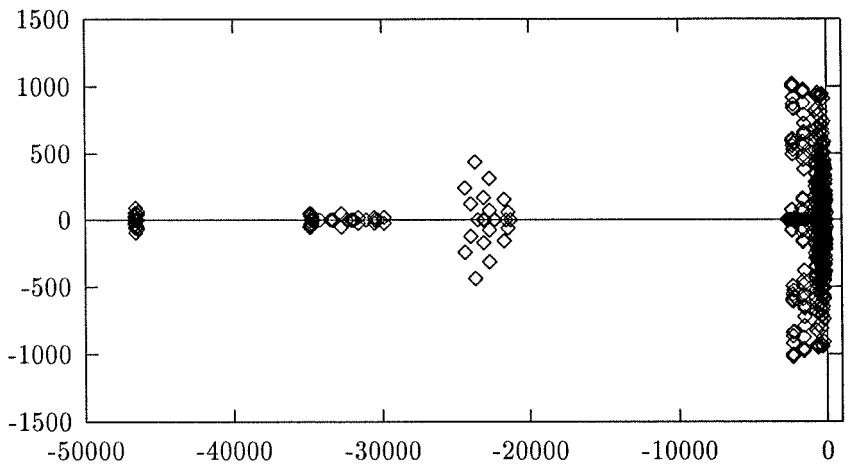

Figure 3.20: The eigenvalues nearest the origin of the upper branch solution.

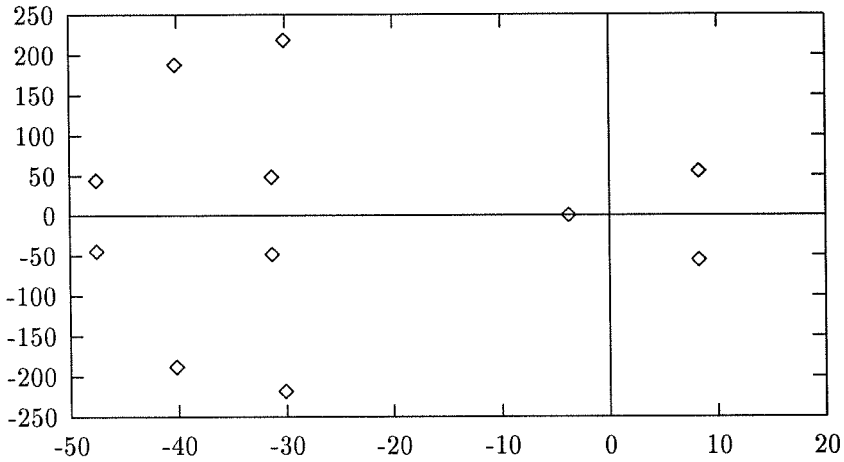

Figure 3.21: The eigenvalues of the upper branch solution has two unstable "Hopf pair" eigenvalues.

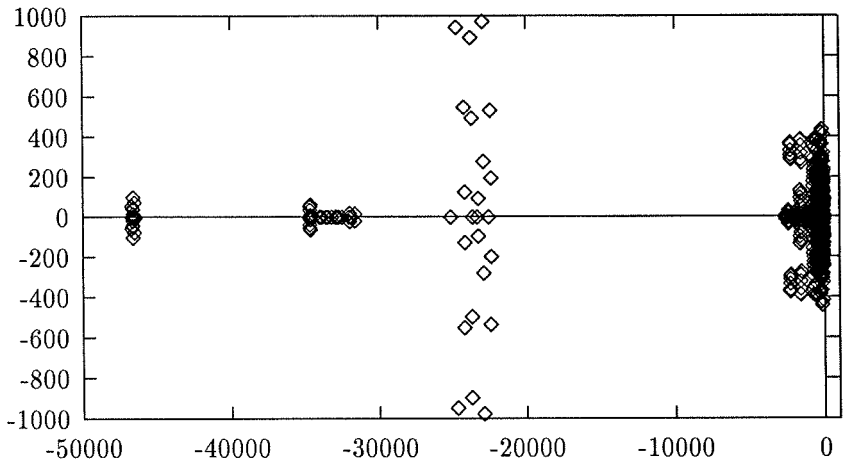

Figure 3.22: The eigenvalues for the solution at $Re = 467, \alpha_y = 0.96, \alpha_z = 2.00$.

values which are nearly zero in Figure 3.23. Note also in Figure 3.22 that the eigenvalues near the imaginary axis have much smaller imaginary parts than the corresponding eigenvalues for other solutions.

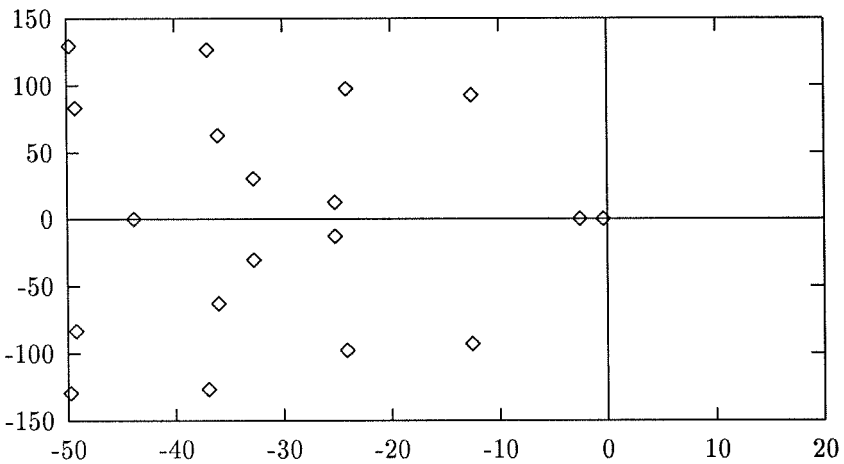

Figure 3.23: The eigenvalues nearest the origin for the solution at $Re = 467, \alpha_y = 0.96, \alpha_z = 2.00$.

Chapter 4

Pressure Driven Flows

There are two canonical plane shear problems. One problem is plane Couette flow in which the flow is driven by the bounding walls. In contrast, plane Poiseuille flow is the flow between stationary walls. The driving force for Poiseuille flow is a pressure gradient parallel to the walls. In the sections below, we try to find a connection between the flows. In order to make the connection between Couette flow and Poiseuille flow, we look for solutions of Eqs. (1.9–1.16) with F_y and F_z nonzero. Note that in this section we use the full set of equations and variables described in Chapter 2 and summarized in Section 2.2. We cannot use the symmetry discussed in Section 2.4.3.

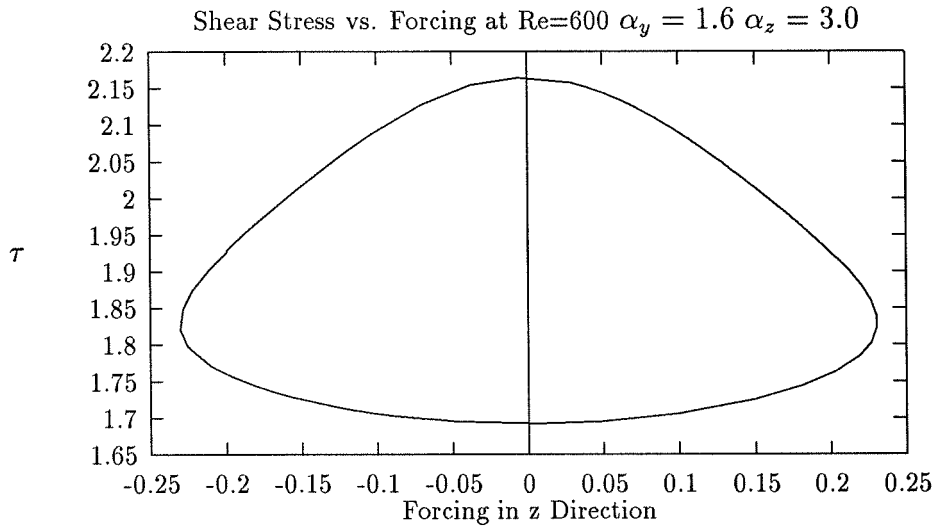

Figure 4.1: Shear Stress vs Forcing in z. Note that the solutions on the upper and lower branch of the solution are connected by the forcing manifold.

4.1 Forcing of Wavy Vortices

In this case, we wish to find solutions of the equations,

$$0 = -\mathrm{Re}\,(\vec{V}\cdot\vec{\nabla})\vec{V} + \nabla^2\vec{V} - \vec{\nabla}p + F_z\hat{z} + c_z\partial_z\vec{V}, \tag{4.1}$$

$$0 = \vec{\nabla}\cdot\vec{V}. \tag{4.2}$$

In one study, we take the lower branch wavy vortex solution at $\Omega = 0$ (see Figure 3.4) and continue in F_z. We use the methods of Chapter 2 to follow the solution path shown in Figure 4.1 which relates shear stress to force. The solution path connects the lower branch solution and the upper branch solution of Figure 3.4. The forcing in the z direction leads to traveling wave

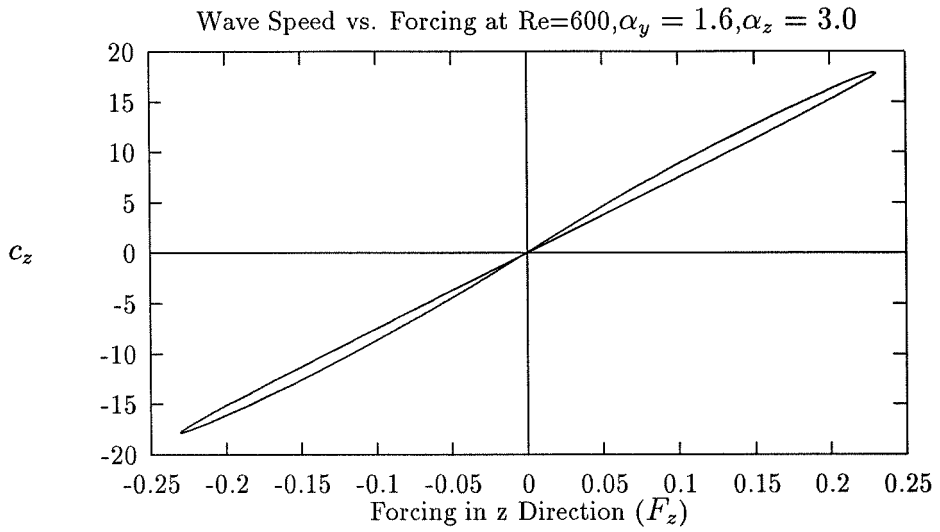

Figure 4.2: Wave speed vs Forcing in 3-D flow at Re=600 $\alpha_y = 1.6$ $\alpha_z = 3.0$ and resolution of (14,3,3).

solutions. The wave speeds, c_z, are shown in Figure 4.2. Poiseuille flow is defined as flow between stationary walls. In this case, as we decrease the wall velocities, V_0, (given in the boundary conditions (1.11–1.12)), the fold points in Figure 4.1 approach the central axis. As a result, we find no simple connection between Couette flow and Poiseuille flow with these solutions.

4.2 Poiseuille Flow with a Coriolis Force

In a similar attempt to find wavy vortices in Poiseuille flow, we start with Poiseuille flow and add a Coriolis force.

$$\begin{aligned} 0 &= -\,\mathrm{Re}\,(\vec{V}\cdot\vec{\nabla})\vec{V} + \nabla^2\vec{V} - \vec{\nabla}p + 2\Omega(\hat{z}\times\vec{V}) \\ &\quad + F_y\hat{y} + c_y\partial_y\vec{V}, \qquad (4.3) \\ 0 &= \vec{\nabla}\cdot\vec{V}. \qquad (4.4) \end{aligned}$$

While these equations (with $F_y = 8, \Omega = 0$) are known to have Tollmein–Schlichting wave solutions for large Reynolds numbers (see [2]), these waves only exist for Reynolds numbers greater than the experimentally observed (turbulent) transition Reynolds number. We attempt to find new solutions to Eq. 4.3 with $\Omega = 0$ by looking for intermediate solutions having non-zero Ω (just as we did for Couette flow in Chapter 3). This problem can be seen as the thin gap limit of flow between concentric rotating cylinders with an azimuthal pressure gradient (otherwise known as the Taylor–Dean problem). (See Appendix A.)

We start with Poiseuille flow ($Re = 600, \Omega = 0, F_y = 8$) and increase Ω. As in Couette flow, Poiseuille flow bifurcates to a two-dimensional flow as the Coriolis force, Ω, is increased. The critical value of Ω is shown in Figure 4.3 as a function of α_z. We switch solution branches using the methods of Chapter 2. The new branch of solutions only varies in the z and x directions. Just as in Couette flow, this two-dimensional flow is not a function of the y variable.

At Reynolds number 600, we see in Figure 4.3 that the minimum Ω for the

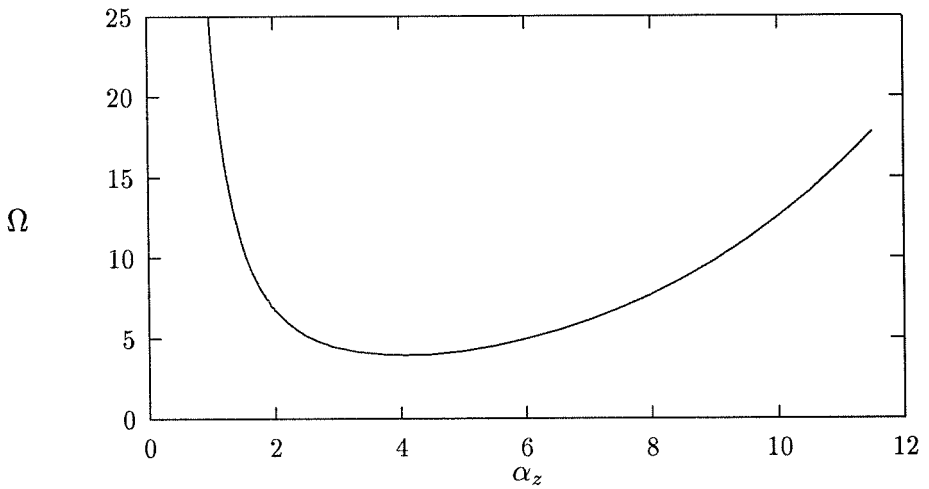

Figure 4.3: The critical Ω as a function of α_z at Reynolds number 600 with 32 Chebyshev polynomials in the x direction. This is Poiseuille flow with the forcing in the y direction. $F_y = 8$.

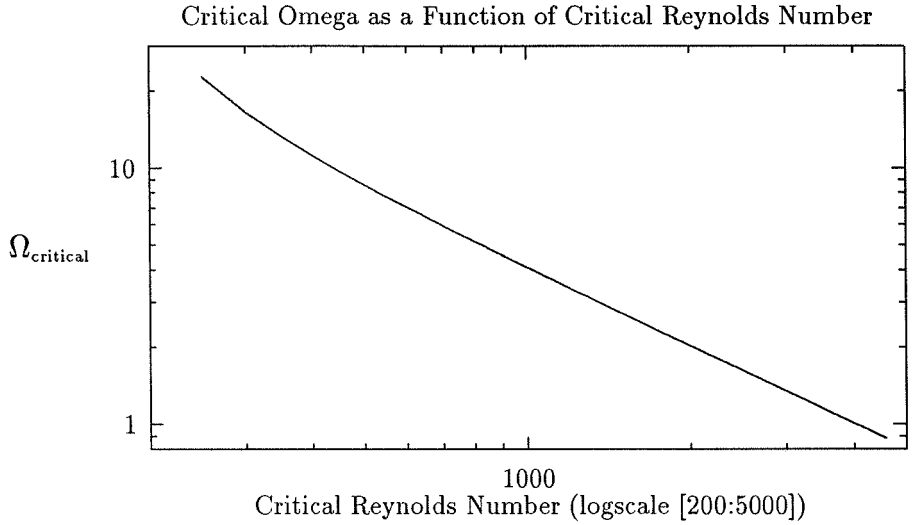

Figure 4.4: Critical Reynolds number vs Critical Ω with 32 Chebyshev polynomials. $F_y = 8, \alpha_z = 1.96$.

bifurcation is found when the wavelength in the z direction is around $2\pi/4$. The value of critical Ω varies with the Reynolds number. In Figure 4.4, we show the relation between the critical Ω and the Reynolds number.

At the critical Ω we switch branches of the solution. We follow the path of solutions for increasing Ω. As in the case of the vortex branch of Couette flow, we graph the shear stress at the wall as a function of Ω in Figure 4.5. We find no bifurcations along this path of solutions; however, there may be a Hopf bifurcation which we do not attempt to find.

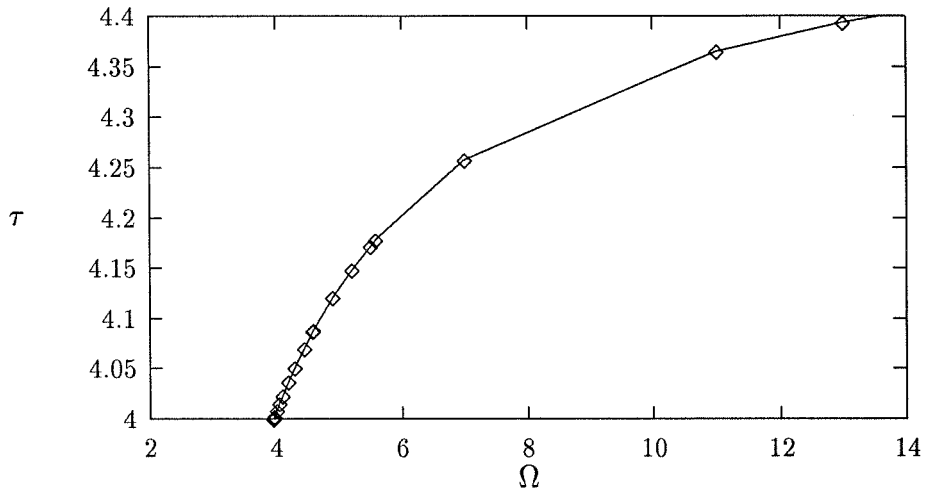

Figure 4.5: Shear Stress (τ) as a function of Rotation (Ω). $Re = 600, F_y = 8, \alpha_z = 4.0, L = 16, N = 4$. The boxes are calculated values along the path. Poiseuille flow has a constant shear stress ($\tau = 4$).

Chapter 5

Discussion

Nagata [8] finds new solutions to the equations for plane Couette flow by introducing a Coriolis force. By varying the Coriolis force, he finds bifurcations from Couette flow to two–dimensional (vortex) solutions and secondary bifurcations to three–dimensional (wavy vortex) solutions. He finds that these three–dimensional solutions persist when the Coriolis force is zero. Using a different approximation scheme in a primitive variable formulation, we confirm these solutions.

Two criticisms of these solutions have been raised by experimenters [10]. The first criticism is of the resolution of Nagata's solutions. We find that these solutions exist at relatively high resolutions (see Table 3.2). The second criticism is a question about the stability of these solutions. We find that these solutions are not stable; however, there may be values of the parameters, Re, α_y, and α_z, for which the solutions are stable (see Figures 3.17, 3.19, 3.21, and 3.23).

In addition to the confirmation of the solutions and the stability computations, we are able to compute several other quantities of interest. In particular, we compute the minimum Reynolds number at which the solutions exist. This allows us to postulate that there are no wavy vortex solutions for Reynolds numbers less than 467.

Along the path of solutions connecting Couette flow and wavy vortices is a path of vortices (see Figure 3.4). We find evidence (see Figure 3.7) that the vortex branch of solutions reconnects with the Couette flow branch at higher Coriolis forces. This indicates that in an experiment, as the Coriolis force, Ω, is increased, we would expect to see Couette flow bifurcate to vortices and the vortices to subsequently bifurcate back to Couette flow. The Taylor number at both bifurcations from Couette flow to vortices and from vortices to Couette flow are the same.

In an attempt to find a connection between the wavy vortex solutions and nontrivial plane Poiseuille flow, we add a force to the wavy vortices at $\Omega = 0$. Following the path of wavy vortices for increasing force leads us to a fold point. This means there are no (steady) solutions for larger forcing.

In another attempt to find wavy vortices in plane Poiseuille flow, we start with the trivial (parabolic profile) Poiseuille flow and add a Coriolis force. We detect and follow a bifurcating branch of vortex solutions. We detect no secondary bifurcations from this branch, but we do not search for Hopf bifurcations. (We would expect a Hopf bifurcation since there is a net flux of fluid in the direction of the forcing.)

We conclude by asking some of the many questions left open by this work. Are there parameter values (Re, α_y, α_z) for which the wavy vortex

solutions are stable? Are there other branches of solutions (see Section 3.1.1) which lead to stable branches of solutions? Is it possible that new solutions appear at $Re \doteq 1440$ (the experimental critical Reynolds number) which help to explain turbulent flows? Can we detect a Hopf bifurcation on the upper branch solution between the fold point and $\Omega = 0$? Is there a Hopf bifurcation leading to a steady three–dimensional flow (at $\Omega = 0$) in plane Poiseuille flow?

Appendix A

Relation to Taylor–Couette Flow and Poiseuille Flow

A.1 Taylor–Couette Flow

Taylor–Couette flow is the flow between concentric cylinders. If the gap width, a, between the cylinders is negligible compared to the average of the radii of the cylinders, b, then the equations governing Taylor–Couette flow are approximately the same as the equations for flow between parallel plates in a rotating frame. We study this limit in this section.

The Incompressible Navier Stokes equations in cylindrical coordinates are:

$$\frac{\partial V_\rho}{\partial \tau} + (\vec{V}\cdot\vec{\nabla})V_\rho - \frac{{V_\theta}^2}{\rho} = -\frac{\partial P}{\partial \rho} + \nu(\nabla^2 V_\rho - \frac{2}{\rho^2}\frac{\partial V_\theta}{\partial \theta} - \frac{V_\rho}{\rho^2}), \quad \text{(A.1)}$$

$$\frac{\partial V_\theta}{\partial \tau} + (\vec{V}\cdot\vec{\nabla})V_\theta + \frac{V_\rho V_\theta}{\rho} = -\frac{1}{\rho}\frac{\partial P}{\partial \theta} + \nu(\nabla^2 V_\theta + \frac{2}{\rho^2}\frac{\partial V_\rho}{\partial \theta} - \frac{V_\theta}{\rho^2}), \quad \text{(A.2)}$$

$$\frac{\partial V_\zeta}{\partial \tau} + (\vec{V}\cdot\vec{\nabla})V_\zeta = -\frac{\partial P}{\partial \zeta} + \nu(\nabla^2 V_\zeta), \tag{A.3}$$

$$0 = \vec{\nabla}\cdot\vec{V} = \frac{1}{\rho}(\frac{\partial}{\partial \rho}(\rho V_\rho)) + \frac{1}{\rho}(\frac{\partial V_\theta}{\partial \theta}) + \frac{\partial V_\zeta}{\partial \zeta}, \tag{A.4}$$

where

$$\vec{V}\cdot\vec{\nabla} = V_\rho\frac{\partial}{\partial \rho} + \frac{V_\theta}{\rho}\frac{\partial}{\partial \theta} + V_\zeta\frac{\partial}{\partial \zeta},$$

$$\nabla^2 = \frac{1}{\rho}\frac{\partial}{\partial \rho}(\rho\frac{\partial}{\partial \rho}) + \frac{1}{\rho^2}\frac{\partial^2}{\partial \theta^2} + \frac{\partial^2}{\partial \zeta^2}.$$

The domain is

$$\rho \in [R_0, R_1],\ \theta \in [-\infty, \infty],\ \zeta \in [-\infty, \infty],$$

and boundary conditions are

$$\vec{V}(R_0, \theta, \zeta, \tau) = V_0\hat{\theta}, \vec{V}(R_1, \theta, \zeta, \tau) = V_1\hat{\theta}, \tag{A.5}$$

where $\hat{\theta}$ is the unit vector in the θ direction.

A.2 Change of Variables

We change variables, using the width of the gap, a, between the cylinders as the length scale. The time scale is a^2/ν. The velocity scale ($\bar{V}$) is chosen later. We also use a new reference frame rotating with the average rotation rate, ω, of the cylinders. Explicitly, the change of variables is as follows:

$$\omega = \frac{V_1 + V_0}{2b},$$

$$b = \frac{R_1 + R_0}{2}, a = R_1 - R_0,$$

$$x = \frac{\rho - b}{a}, y = \frac{b(\theta - \omega\tau)}{a}, z = \frac{\zeta}{a},$$
$$t = \frac{\nu\tau}{a^2},$$
$$\bar{V}\vec{u}(x,y,z,t) = \vec{V}(\rho,\theta,\zeta,\tau) - \rho\omega\hat{\theta},$$
$$\frac{\nu\bar{V}}{a}p = P - \frac{\omega^2}{2}\rho^2,$$

where

$$\vec{V} = \begin{pmatrix} V_\rho \\ V_\theta \\ V_\zeta \end{pmatrix}, \vec{u} = \begin{pmatrix} u \\ v \\ w \end{pmatrix}.$$

The Navier Stokes equations become:

$$\begin{aligned} u_t &= -\mathrm{Re}\left[(\vec{u}\cdot\vec{\nabla})u - \frac{\epsilon v^2}{1+\epsilon x}\right] + 2\Omega v - \frac{\partial p}{\partial x} \\ &\quad +(\nabla^2 u - \frac{2\epsilon}{(1+\epsilon x)^2}\frac{\partial v}{\partial y} - \frac{\epsilon^2}{(1+\epsilon x)^2}u), \qquad \text{(A.6)} \\ v_t &= -\mathrm{Re}\left[(\vec{u}\cdot\vec{\nabla})v + \frac{\epsilon uv}{1+\epsilon x}\right] - 2\Omega u - \frac{1}{1+\epsilon x}\frac{\partial p}{\partial y} \\ &\quad +(\nabla^2 v + \frac{2\epsilon}{(1+\epsilon x)^2}\frac{\partial u}{\partial y} - \frac{\epsilon^2}{(1+\epsilon x)^2}v), \qquad \text{(A.7)} \\ w_t &= -\mathrm{Re}\left[(\vec{u}\cdot\vec{\nabla})w\right] - \frac{\partial p}{\partial z} \\ &\quad +(\nabla^2 w), \qquad \text{(A.8)} \\ 0 &= \vec{\nabla}\cdot\vec{u} = \frac{\partial u}{\partial x} + \frac{\epsilon}{1+\epsilon x}u + \frac{1}{1+\epsilon x}\frac{\partial v}{\partial y} + \frac{\partial w}{\partial z}, \qquad \text{(A.9)} \end{aligned}$$

where

$$\begin{aligned} \vec{u}\cdot\vec{\nabla} &= u\frac{\partial}{\partial x} + \left(\frac{1}{1+\epsilon x}\right)v\frac{\partial}{\partial y} + w\frac{\partial}{\partial z}, \\ \nabla^2 &= \frac{\partial^2}{\partial x^2} + \frac{1}{(1+\epsilon x)^2}\frac{\partial^2}{\partial y^2} + \frac{\partial^2}{\partial z^2} + \frac{\epsilon}{1+\epsilon x}\frac{\partial}{\partial x}, \end{aligned}$$

$$\epsilon = \frac{a}{b}, \qquad \Omega = \tfrac{a^2}{\nu}\omega, \qquad \mathrm{Re} = \frac{\bar{V}a}{\nu},$$
$$x \in [-1/2, 1/2], \quad y \in [-\infty, \infty], \quad z \in [-\infty, \infty].$$

The boundary conditions are the following:

$$u(\pm 1/2, y, z, t) = 0, \tag{A.10}$$
$$v(\pm 1/2, y, z, t) = \pm\frac{1}{2}\left(\frac{V_1 - V_0}{\bar{V}}\right) \mp \frac{\Omega}{2\mathrm{Re}}, \tag{A.11}$$
$$w(\pm 1/2, y, z, t) = 0. \tag{A.12}$$

A.3 Thin–gap Limit

In the limit $\epsilon \to 0$, these equations reduce to the Cartesian equations satisfied by a fluid between parallel plates in a rotating frame:

$$\vec{u}_t = -\mathrm{Re}(\vec{u}\cdot\vec{\nabla})\vec{u} - 2\Omega(\hat{z}\times\vec{u}) - \vec{\nabla}p + \nabla^2\vec{u}, \tag{A.13}$$
$$0 = \vec{\nabla}\cdot\vec{u} = \frac{\partial u}{\partial x} + \frac{\partial v}{\partial y} + \frac{\partial w}{\partial z}, \tag{A.14}$$

where

$$\vec{u}\cdot\vec{\nabla} = u\frac{\partial}{\partial x} + v\frac{\partial}{\partial y} + w\frac{\partial}{\partial z},$$
$$\nabla^2 = \frac{\partial^2}{\partial x^2} + \frac{\partial^2}{\partial y^2} + \frac{\partial^2}{\partial z^2}.$$

The rotation, Ω, is about the z–axis which is the axis of rotation of the cylinders. The boundary conditions are the following:

$$u(\pm 1/2, y, z, t) = 0, \tag{A.15}$$

$$v(\pm 1/2, y, z, t) = \pm\frac{1}{2}\left(\frac{V_1 - V_0}{\bar{V}}\right) \mp \frac{\Omega}{2\mathrm{Re}}, \tag{A.16}$$

$$w(\pm 1/2, y, z, t) = 0. \tag{A.17}$$

Plane Couette Flow and Plane Poiseuille Flow

Equations A.13–A.17 include two separate special cases. When

$$\Omega = 0, \bar{V} = V_1 - V_0,$$

the equations are satisfied by plane Couette flow. When

$$\Omega = 0, V_0 = V_1 = 0,$$

$$p(x, y, z, t) = F_y y + p'(x, y, z),$$

$$p'(x, y + \lambda_y, z) = p'(x, y, z),$$

$$p'(x, y, z + \lambda_z) = p'(x, y, z),$$

and $\bar{V}$ is the average (over y and z) of $v(0, y, z, t)$, the equations are satisfied by plane Poiseuille flow with the driving pressure gradient in the y–direction (i.e., the transformed θ–direction.)

Appendix B

Singular Points in the Linear Stability Analysis of Plane Shear Flows

In this section we study some of the singular points of the linearized equations for shear flows between parallel plates in a rotating frame. In particular, we show that the Taylor number (T) arises naturally in linear stability analysis.

We start with the Navier–Stokes equations linearized about a shear flow $(\vec{V}, p)$; that is, we seek flows of the form $(\vec{V} + \vec{\epsilon}, p + \rho)$ where $\vec{V}$ only varies with x and $\vec{\epsilon}$ is "small." Dropping quadratic terms in $\vec{\epsilon}$ we get:

$$0 = -\mathrm{Re}((\vec{V} \cdot \vec{\nabla})\vec{\epsilon} + (\vec{\epsilon} \cdot \vec{\nabla})\vec{V}) - 2\Omega(\hat{z} \times \vec{\epsilon}) - \vec{\nabla}\rho + \nabla^2\vec{\epsilon}, \quad \text{(B.1)}$$

$$0 = \vec{\nabla} \cdot \vec{\epsilon}, \quad \text{(B.2)}$$

where

$$\vec{\epsilon}(\pm 1/2, y, z) = 0. \tag{B.3}$$

We seek solutions in the form,

$$\vec{\epsilon} = \begin{pmatrix} \epsilon_x(x)cos(\alpha z), \\ \epsilon_y(x)cos(\alpha z) \\ \epsilon_z(x)sin(\alpha z) \end{pmatrix},$$

$$\rho = \rho(x)cos(\alpha z),$$

$$\vec{V} = V(x)\hat{y}.$$

Equations (B.1)–(B.3) then imply

$$\begin{aligned} \epsilon_z &= -\frac{1}{\alpha}\frac{\partial \epsilon_x}{\partial x}, \\ \epsilon_y &= -\frac{1}{2\Omega\alpha^2}(\frac{\partial^2}{\partial x^2} - \alpha^2)\epsilon_x, \\ \rho &= \frac{1}{\alpha^2}(\frac{\partial^2}{\partial x^2} - \alpha^2)\frac{\partial \epsilon_x}{\partial x}, \end{aligned}$$

and ϵ_x must satisfy the linear eigenvalue problem,

$$0 = (\mathrm{Re}\frac{\partial V}{\partial x} - 2\Omega)(2\Omega)\alpha^2\epsilon_x + (\frac{\partial^2}{\partial x^2} - \alpha^2)^3\epsilon_x, \tag{B.4}$$

$$\epsilon_x(\pm 1/2) = \frac{\partial}{\partial x}(\epsilon_x)(\pm 1/2) = (\frac{\partial^2}{\partial x^2} - \alpha^2)^2(\epsilon_x)(\pm 1/2) = 0. \tag{B.5}$$

In the particular case of Couette flow ($V(x) = x$,) equation B.4 reduces to

$$0 = T\alpha^2\epsilon_x + (\frac{\partial^2}{\partial x^2} - \alpha^2)^3\epsilon_x, \tag{B.6}$$

where

$$T = 2\Omega(\mathrm{Re} - 2\Omega). \tag{B.7}$$

This shows that the Taylor number T arises naturally in the linear stability analysis of Couette flow.

Bibliography

[1] Canuto, Hussaini, Quarteroni, and Zang. *Spectral Methods in Fluid Dynamics.* Springer-Verlag, 1988.

[2] P. G. Drazin and W. H. Reid. *Hydrodynamic Stability.* Cambridge University Press, 1981.

[3] D. Gottlieb and S. A. Orszag. *Numerical Analysis of Spectral Methods: Theory and Applications.* SIAM-CBMS, Philadelphia, 1977.

[4] H. B. Keller. *Numerical Methods in Bifurcation Problems.* Springer-Verlag, 1987.

[5] Anders Lundbladh and Arne V. Johansson. Direct simulation of turbulent spots in plane Couette flow. *J. Fluid Mech.*, 229:499–516, 1991.

[6] M. Nagata. Bifurcations in Couette flow between almost corotating cylinders. *J. Fluid Mech.*, 169:229–250, 1986.

[7] M. Nagata. On wavy instabilities of the Taylor-vortex flow between corotatng cylinders. *J. Fluid Mech.*, 188:585–598, 1988.

[8] M. Nagata. Three-dimensional finite-amplitude solutions in plane Couette flow: bifurcation from infinity. *J. Fluid Mech.*, 217:229–250, 1990.

[9] V. A. Romanov. Stability of plane parallel Couette flow. *Functional Anal. and Its Applics*, 7:137–146, 1973.

[10] Nils Tillmark and P. Henrik Alfredsson. Experiments on transition in plane Couette flow. *J. Fluid Mech.*, 235:89–102, 1992.